



FINAL REPORT

**U.S. DOT
Pipeline and Hazardous
Materials Safety
Administration**

**Competitive Academic
Agreement Program**

**Advancement in the Area of Intrinsically
Locatable Plastic Materials**

West Virginia University

CAAP Final Report

Date of Report: September 29, 2017

Contract Number: *DTPH5615HCAP09*

Prepared for: U.S. Department of Transportation/Pipeline and Hazardous Materials Safety Administration (USDOT-PHMSA)

Project Title: Advancement in the Area of Intrinsically Locatable Plastic Materials

Prepared by: West Virginia University, Constructed Facilities Center (WVU-CFC)

Project PI/co-PI: Udaya B. Halabe, Hota V. S. GangaRao, John Zondlo

Graduate Students: Jonas Kavi, Ben Imes, Andrew Cvetnick

Contact Information: Dr. Udaya B. Halabe, Professor, CEE Department, WVU

Email: Udaya.Halabe@mail.wvu.edu

Phone: 304-293-9934

Project ending date: *September 29, 2017*

Acknowledgement

This project is funded by USDOT-PHMSA's Competitive Academic Agreement Program (Project # DTPH5615HCAP09).

Executive Summary

Pipelines are crucial in transporting petroleum products and natural gas from production facilities to consumers. The important role played by energy pipelines in the US economy and standard of living of citizens requires that these assets be safely maintained and appropriately expanded to meet growing demand.

Pipelines remain the safest means of transporting natural gas and petroleum products, nonetheless, the pipeline infrastructure in the US is facing major challenges, especially, corrosion of steel/metallic pipes (leading to oil spills, explosions and deaths) and excavation damage of onshore pipelines. Problems associated with corrosion of metallic pipelines can be avoided by using non-corrosive materials such as the commonly available and widely used PVC (Polyvinyl Chloride) for water/sewer lines and Glass Fiber Reinforced Polymer composite (GFRP) for transporting high-pressure oil and natural gas. But buried GFRP and PVC material are not easily detectable using the traditional techniques used by construction crews to detect buried metallic pipes, which can lead to increased excavation damage during building/construction and rehabilitation works.

This research project has investigated and developed GFRP pipes capable of resisting high burst pressures. In addition, this research has investigated and compared alternative strategies for locating buried CFRP, GFRP, and PVC pipes that will help address the detection of these nonmetallic pipes. Nondestructive testing methods such as Ground Penetrating Radar (GPR), Infrared Thermography (IRT), and Mass Spectroscopy were utilized for pipe material detection and leak detection in this project.

Results from this research have shown that, using carbon fabric and aluminum foil overlay on non-metallic GFRP or PVC pipes before burying significantly increases the reflected GPR signal, thereby making it easier to locate such pipelines using GPR. This research involved pipes up to 12 inch diameter and depths up to 4 ft. The results also show great potential for using IRT to detect buried pipelines carrying hot liquids, by measuring temperature difference at the soil surface. In addition, gas leak detection using Mass Spectrometer has been investigated as a means of locating buried pipes, which can also lead to timely repair of areas with gas leakage.

Table of Contents

CAAP Final Report	ii
Acknowledgement	iii
Executive Summary	iv
Table of Contents	v
List of Figures.....	vii
List of Tables	x
1 INTRODUCTION	1
1.1 Background.....	1
1.2 Research Objectives	3
2 FRP PIPE DEVELOPMENT	4
2.1 FRP Properties	4
2.2 Manufacturing of FRP Pipe	4
2.2.1 Pultrusion	5
2.2.2 Filament Winding.....	6
2.2.3 Pull-Winding.....	7
2.3 Development Manufacturing and Testing of Joints	7
2.4 Testing of Pipes	9
2.4.1 Pultruded Pipe Tests.....	9
2.4.2 Pultruded Pile Tests	10
2.4.3 Filament Wound Pipe Tests	12
2.5 Conclusions	13
3 PIPE SET UP FOR GPR TESTING.....	14
3.1 Introduction	14
3.2 Pipe Preparation.....	14
3.2.1 PVC pipes	14
3.2.2 GFRP pipes	15
3.2.3 CFRP pipes	17
3.2.4 Using CFRP fabric and aluminum foil tape to make non-metallic pipes detectable.....	18
3.3 Pipe Burying	20

3.4	Conclusions	23
4	GPR TESTS AND RESULTS	24
4.1	Introduction	24
4.2	GPR Equipment	24
4.3	GPR Test Results	25
4.4	Conclusions	40
5	IRT TEST SET UP AND RESULTS	41
5.1	Introduction	41
5.2	IRT Camera and Thermocouples	41
5.3	Experimental Set-Up for IRT Testing	42
5.4	IRT Test Results	44
5.5	Conclusions	47
6	GAS LEAK TESTING	49
6.1	Introduction	49
6.2	Test Set-Up	49
6.3	Test Results	54
6.4	Conclusions	58
7	BROADER IMPACTS	59
8	CONCLUSIONS.....	60
	REFERENCES.....	62

List of Figures

Figure 1-1: (a) 2014 U.S. Primary energy consumption by source (EIA) and (b) 2009 crude oil and petroleum products by transportation mode (USDOT)	1
Figure 2-1: Pultrusion Machine.....	5
Figure 2-2: Filament Winding Machine	6
Figure 2-3: Pull-winding Machine	7
Figure 2-4: Filament Wound Sleeve Joint	8
Figure 2-5: Heat Fusion Joint	9
Figure 2-6: Load Resisting System.....	10
Figure 2-7: Pultruded Pile.....	11
Figure 2-8: Eccentricity and Endcap Rotation	12
Figure 2-9: Filament Wound Pipe	13
Figure 3-1: The 12" diameter PVC pipe (a) after cutting, and (b) after capping.....	15
Figure 3-2: The 3" diameter PVC pipes	15
Figure 3-3: The 12" diameter GFRP pipes.....	16
Figure 3-4: 3" diameter GFRP pipes (a), (b) manufacturing process, and (c) a completed pipe	17
Figure 3-5: 12" diameter CFRP pipe	18
Figure 3-6: The 3" diameter CFRP pipes.....	18
Figure 3-7: Completed (wrapped) pipes: (a) 6" diameter PVC with carbon fabric rings, (b) 12" diameter PVC with carbon fabric strip, (c) 12" diameter GFRP with aluminum rings, and (d) 12" diameter GFRP with aluminum strip	19
Figure 3-8: The located site within WVU campus for burying the pipes	20
Figure 3-9: Pipe layout for GPR testing.....	21
Figure 3-10: (a) Arrangement of pipes in the trench, (b) soil moisture and resistivity sensor	22
Figure 3-11: 12" and 6" diameter pipes being buried	22
Figure 3-12: (a) The site being seeded, (b) the field restored to initial condition.....	23
Figure 4-1: SIR-20 GPR system and antennae used for testing	24
Figure 4-2: 200 MHz GPR antenna with survey wheel.....	25
Figure 4-3: Longitudinal and transverse scans over the trenches using 400 MHz GPR antenna	26

Figure 4-4: Close up views of scans over 3" diameter pipes using 400 MHz GPR antenna	27
Figure 4-5: Dataset II - Longitudinal scans along the full length pipe trenches using 200 MHz GPR antenna.....	29
Figure 4-6: Dataset II - Longitudinal scan and the processed data along the full length of 3 ft. deep trench	30
Figure 4-7: Dataset II - Longitudinal scan and the processed data along the full length of 4 ft. deep trench	30
Figure 4-8: Dataset II - Longitudinal scan and the processed data along the full length of 2 ft. deep trench	31
Figure 4-9: Dataset III - Longitudinal scan and the processed data along the full length of 3 ft. deep trench	32
Figure 4-10: Dataset III - Longitudinal scan and the processed data along the full length of 4 ft. deep trench	32
Figure 4-11: Dataset III - Longitudinal scan and the processed data along the full length of 2 ft. deep trench	33
Figure 4-12: Longitudinal GPR scan (left) and A-Scan (right) over 12" Unwrapped GFRP pipe	34
Figure 4-13: Longitudinal GPR scan (left) and A-Scan (right) over 12" CFRP Ring GFRP pipe	35
Figure 4-14: Longitudinal GPR scan (left) and A-Scan (right) over 12" CFRP Strip GFRP pipe	35
Figure 4-15: Longitudinal GPR scan (left) and A-Scan (right) over Unwrapped 12" PVC pipe.	36
Figure 4-16: Longitudinal GPR scan (left) and A-Scan (right) over Al. Foil Ring 12" PVC pipe	36
Figure 4-17: Longitudinal GPR scan (left) and A-Scan (right) over Al. Foil Strip 12" PVC pipe	37
Figure 4-18: Longitudinal GPR scan (left) and A-Scan (right) over Unwrapped 6" PVC pipe...	37
Figure 4-19: Longitudinal GPR scan (left) and A-Scan (right) over Al. Foil Ring 6" PVC pipe.	38
Figure 4-20: Longitudinal GPR scan (left) and A-Scan (right) over Al. Foil Strip 6" PVC pipe.	38
Figure 4-21: Longitudinal GPR scan (left) and A-Scan (right) over CFRP Ring 6" PVC pipe...	39
Figure 4-22: Longitudinal GPR scan (left) and A-Scan (right) over CFRP Strip 6" PVC pipe...	39

Figure 5-1: FLIR InfraCAM SD camera and type-T thermocouple.....	41
Figure 5-2: Insulated wooden box used for IRT testing	43
Figure 5-3: Capped CFRP pipe used for IRT testing.....	43
Figure 5-4: IRT test set-up.....	44
Figure 5-5: Infrared thermography data at the soil surface at various stages of testing	45
Figure 5-6: Variation of soil surface (TSC, IRT) and room (Amb) temperatures with time	46
Figure 5-7: Soil surface temperature difference with time.....	46
Figure 5-8: Difference between soil surface temperature and room temperature with depth	48
Figure 6-1: (a) New wooden box, showing caulked seams, (b) Interior of assembled box, and (c) Exterior of assembled box.....	50
Figure 6-2: CO ₂ Cylinder and Pressure Regulator	51
Figure 6-3: (a) Testing apparatus schematic diagram side view, (b) Testing apparatus schematic diagram end view, and (c) Testing apparatus schematic, interior view	52
Figure 6-4: Mass spectrometer and associated experimental equipment.	53
Figure 6-5: Concentration of CO ₂ as a function of time for a leak in the test pipe (expressed as arbitrary pressure)	54
Figure 6-6; (a), (b), (c), (d): All represent the titles given to each with the starting pressure for the shown trial listed after the trial number. The slope of the best fit lines represents the experimental “k” values mentioned in the text above.	57

List of Tables

<i>Table 2-1: Material Stiffness and Strength</i>	<i>4</i>
<i>Table 3-1: Material and section properties of CFRP and GFRP pipes/fabrics used</i>	<i>16</i>
<i>Table 4-1: Average soil dielectric constant during data collection</i>	<i>28</i>

1 INTRODUCTION

1.1 Background

Over 3 million miles of oil, gas, water, and sewage pipelines in the United States of America are the backbone of our economic well-being, and arterial network of modern living in comfort. Oil and gas pipelines, especially the distribution systems, have been utilizing materials such as steel, copper, fiber reinforced polymer (FRP) composites and even unreinforced high density polyethylene for low pressure lines. Most of US oil and gas pipelines are buried underground for reasons of safety, resulting in a formal search process, through “The National Pipeline Mapping System” to locate an underground pipeline.

According to data available from the U.S. Energy Information Administration (EIA), the US consumes about 100 quadrillions Btu of energy annually. Natural gas and petroleum products account for about 63% of the total energy consumption. Natural gas is almost exclusively transported by pipelines while over 70% of crude oil and petroleum products are transported by pipelines. Thus, 53% of all energy commodities consumed in the United States are transported by pipelines (EIA n.d., USDOT n.d.).

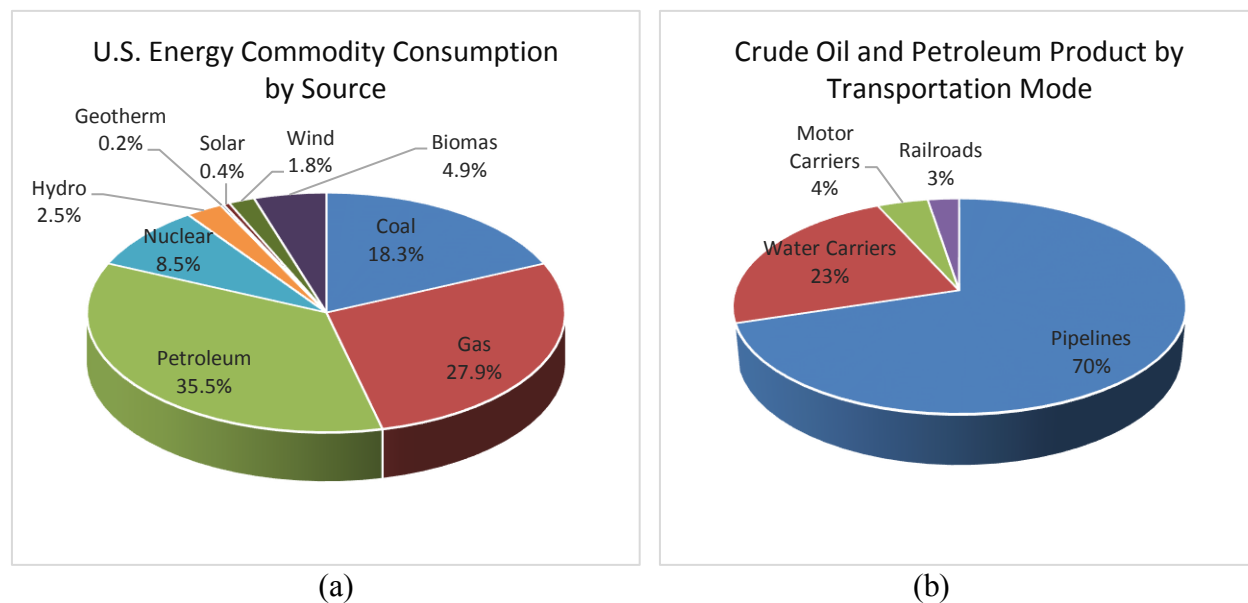


Figure 1-1: (a) 2014 U.S. Primary energy consumption by source (EIA) and (b) 2009 crude oil and petroleum products by transportation mode (USDOT)

The importance of pipelines (particularly energy pipelines) “to the U.S. economy and our standard of living requires that these assets be safely maintained and appropriately expanded to sustain demand.” (PHMSA 2015).

Pipelines remain the safest means of transporting natural gas and petroleum products, nonetheless, the pipeline industry is having major challenges; including corrosion of steel pipes (leading to oil spills, explosions and deaths), excavation damage (damage to existing pipelines during excavation work), and pipeline material/equipment failure. These pipeline incidents often result in catastrophic failures, with associated fatalities, injuries, property loss, and environmental contamination. The Pipeline and Hazardous Materials Safety Administration (PHMSA), under U.S. Department of Transportation (USDOT), has identified corrosion as the leading cause of failure in metallic pipelines, and excavation damage as the leading cause of on shore pipeline incidents (PHMSA 2015).

In May 2015, external corrosion caused the rupture of a 24 inch diameter pipeline in Santa Barbara County, California. This incident resulted in the release of over 2,900 barrels of crude oil that contaminated the surrounding areas, beaches and ocean in addition to the associated cost (PHMSA 2016a and 2016b). Excavation damage mostly results in immediate pipeline failure due to line hits with excavation equipment; however, there have been failures that resulted from mechanical damage inflicted on the pipeline from previous excavation damage (Baker 2009). If excavation damage does not result in immediate pipeline failure, damage to pipeline coating can allow accelerated corrosion to occur; a combination of the resulting corrosion and the physical damage to the pipe material can result in increased potential for future failure. “Unreported mechanical damage can have serious consequences” (Baker 2009).

Issues related to corrosion of steel pipes, and to some extent, pipe material failure can be addressed by using non-metallic advanced composite materials such as Glass Fiber Reinforced Polymer (GFRP). But buried GFRP material is not easily detectable using the available ground sensory technologies, which can lead to increased excavation damage during building/construction and rehabilitation works. Tracer wires are employed in some applications to make non-metallic pipelines locatable, but these wires can break over time and render the pipeline difficult to locate. The inability to easily locate buried GFRP and other non-metallic pipes has limited the adoption of such pipe materials in the oil and gas industry. Making these pipe materials detectable will

therefore help accelerate their adoption, and hence provide solutions to the corrosion related pipeline failure incidents as well. This research has investigated alternative strategies for making buried non-metallic pipeline easily detectable using available ground sensory technologies - Ground Penetrating Radar (GPR) and Infrared Thermography (IRT).

1.2 Research Objectives

To help address some of the major challenges associated with transportation by pipelines, this research aims to produce easily locatable non-metallic pipe materials through the following objectives:

1. Develop, investigate, and compare alternative strategies for creating easily locatable Fiber Reinforced Polymer (FRP) pipes using Carbon and Glass (CFRP and GFRP).
2. Use Aluminum or CFRP fabric overlay for GFRP and PVC (plastic) pipes to increase detectability.
3. Use carbon nanoparticle overly for GFRP pipes to increase detection.
4. Investigate and compare the detectability of the above pipes using Ground Penetrating Radar (GPR).
5. Investigate the possibility of detecting buried pipe transporting hot liquid, using Infrared Thermography (IRT).
6. Investigate the possibility of buried pipe/gas leak detection using Spectroscopy.

2 FRP PIPE DEVELOPMENT

2.1 FRP Properties

Glass Fiber Reinforced Polymer Pipe (GFRP) and Carbon Fiber Reinforced Polymer Pipe (CFRP) have many properties that make it a favorable material for use in natural gas and hazardous liquid pipeline industries. In comparison to steel, the primary material used in transmission lines, FRP has a higher strength to weight to ratio (60-300ksi rupture strength, specific gravity of 1.8), higher flexibility, lower corrosiveness and thermal and electrical conductivity, less susceptibility to hydrogen embrittlement, and costs roughly the same per linear foot of pip. In comparing GFRP and CFRP, CFRP is more expensive, but also has higher strength and stiffness. Carbon is also more electrically conductive than glass. Hence, FRP pipe has the potential to be a replacement of steel as the primary structural material used in gas transmission lines. However, as has been discussed in previous sections, FRP pipe is not inherently detectible unless it is modified through the various processes and shapes as discussed in this report (GangaRao et al. 2016). **Error! eference source not found.** provides comparisons between CFRP, GFRP, Steel and Aluminum alloy for strength, stiffness, and density (Storm).

Table 2-1: Material Stiffness and Strength

PROPERTIES, AND SPECIFIC PROPERTIES, OF COMPOSITES								
Material	Density ρ (Mg m^{-3})	Young's modulus E (GPa)	Strength σ_y (MPa)	Fracture toughness K_{IC} (MPa $\text{m}^{1/2}$)	E/ρ	$E^{1/2}/\rho$	$E^{1/3}/\rho$	σ_y/ρ
<i>Composites</i>								
CFRP, 58% uniaxial C in epoxy	1.5	189	1050	32-45	126	9	3.8	700
GFRP, 50% uniaxial glass in polyester	2.0	48	1240	42-60	24	3.5	1.8	620
Kevlar-epoxy (KFRP), 60% uniaxial Kevlar in epoxy	1.4	76	1240	—	54	6.2	3.0	886
<i>Metals</i>								
High-strength steel	7.8	207	1000	100	27	1.8	0.76	128
Aluminium alloy	2.8	71	500	28	25	3.0	1.5	179

2.2 Manufacturing of FRP Pipe

Carbon and Glass FRP members can be manufactured through a number of different manual and automated processes, such as hand lay-up, pultrusion, filament winding, resin transfer molding, injection molding, and compression molding (GangaRao et al. 2007). Research during this phase of the project has primarily utilized the pultrusion and filament winding processes for

the fabrication of GPFP and CFPR pipes. Additionally, the pull winding process, which is a combination of the pultrusion and filament winding processes, is being evaluated for this sort of application, because of the amenability to mass production of high grade composite parts. While pipes have not yet been fabricated through this method, the process is very promising for application in pressurized pipes. The polymer composite pipes have contained constituent materials such as glass or carbon fabrics and binders such as vinyl ester, polyurethane, and epoxy resins. At this point, the manufacturing has been done by Creative Pultrusion Inc. and Kenway Corporation, a recently acquired subsidiary of Creative Pultrusion Inc., Alum Bank, PA.

2.2.1 Pultrusion

The process of pultrusion involves the pulling of fiber fabrics or fiber rovings through a resin bath and heated die. The fibers are first pulled from creels and run through a resin bath, which could contain wetting agents, fillers, catalysts, accelerators, and pigments. These admixtures affect the curing time, cost, and structural properties of the sections. The fibers are then shaped into a variety of sections by guides along the length of the machine. The fibers are then fed into the heated die, which initiates the cure. After passing through the die, the section is allowed to cool and then is cut to specified length. The output of a pultrusion machine is between 1 and 5 linear feet per minute; however, the throughput speed can be higher depending on the shape being pulled through the die. (GangaRao et al. 2007). **Error! Reference source not found.** below shows a typical configuration of a pultrusion machine.

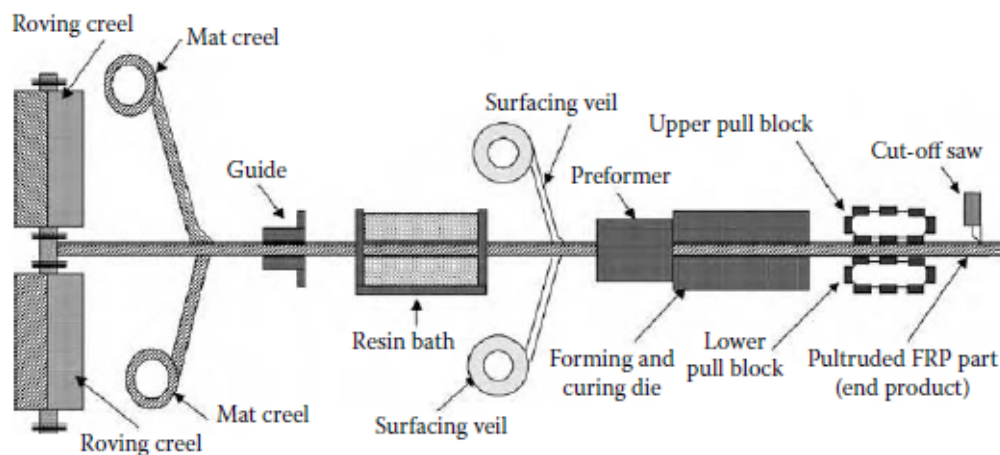


Figure 2-1: Pultrusion Machine

In 2010-2012, WVU-CFC investigated the bending strengths of various sizes of pultruded pipe. 4 different sections were tested: a 1/2" thick 16" outer diameter E-glass/polyurethane, a 1/2" thick 16" outer diameter E-glass/vinyl ester, a 1/2" thick 12" diameter E-glass/polyurethane, and a 3/8" thick E-glass/polyurethane. Numerous tests were conducted on these 4 types of sections: 4 point bending fatigue tests, static load to failure, crush strength tests, washer tests, and transverse bolt tests (Dispennette 2012).

2.2.2 Filament Winding

The process of filament winding involves the wrapping of many continuous strands of fiber or continuous mats around a mandrel. The mandrel is made from one of several different materials, such as plywood, aluminum, and steel. Once again, the fibers are wetted by being run through a resin bath prior to wrapping around the mandrel. The member is then cured through the application of heat lamps or by being fed through an oven. Once curing is initiated, shrink-wraps are employed to minimize voids. Shrink wrap is a flexible, thin plastic that is wrapped around the specimen to provide uniform pressure. The wrap is removed after the curing has finished. A key advantage provided by filament winding is the ability of the process to produce a fabric architecture with fibers running in the magic angle. That is to say that fibers run at plus/minus 54 degrees. This angle is the optimum angle for pipes because the combination of hoop stress and longitudinal stress, created by internal pressures, act along this angle (GangaRao et al. 2007). **Error! Reference source not found.** below shows a typical filament-winding machine.

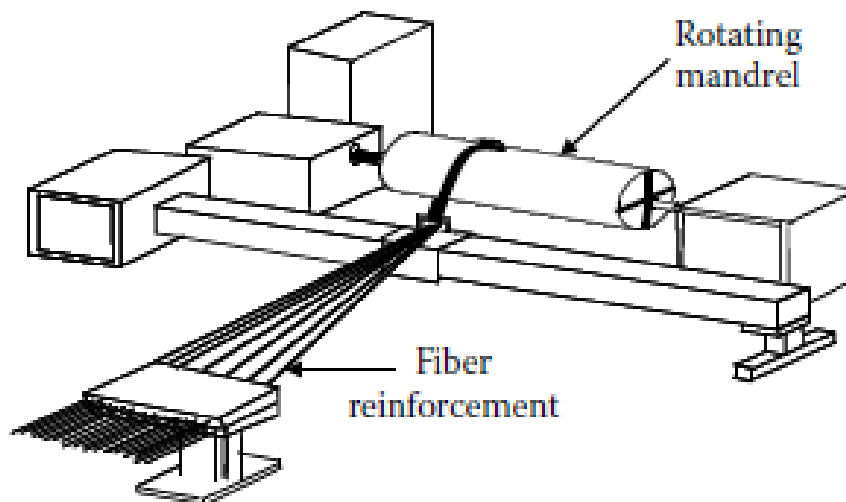


Figure 2-2: Filament Winding Machine

2.2.3 Pull-Winding

The process of pull-winding (Figure 2-3) is a combination of filament winding and pultrusion. A pull winding machine is essentially a pultrusion machine with an independent winding unit. This process allows for the manufacturing of high performance composite tubes. The technique intersperses longitudinal reinforcement layers with helically wound layers. As the longitudinal fibers are pulled through the resin bath towards the die, two winding heads, working in opposite directions, wrap the dry hoop fibers at the desired angle. Once the member is wrapped, it is pulled into the die. The pull-winding process is the best process for the fabrication of pipes designed to resist high internal pressures. It combines the advantages of the previously mentioned processes (Akovali 2001).

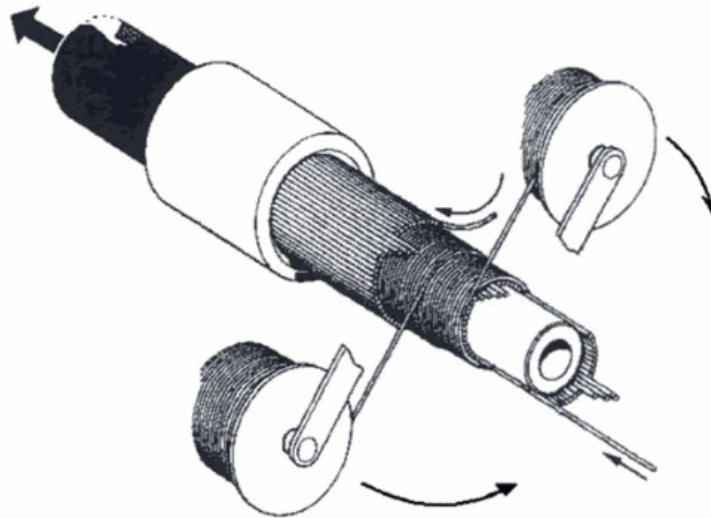


Figure 2-3: Pull-winding Machine

2.3 Development Manufacturing and Testing of Joints

Development of joints has been conducted only at a preliminary level. The main reason for this decision flows from the requirement that the pipes themselves must be able to hold significant pressures (e.g. 2000-4000 psi) before any testing of joints makes sense. Therefore, design and testing of joints will be more thoroughly addressed during the second half of phase 2 of the project (September 2017-September 2018). At this point, two different types of joints are in consideration. The first is known as a filament wound sleeve joint. GangaRao provided a design to Kenway

Corporation in the fall of 2016. In turn, Kenway manufactured 2, 24 inch long pipes, joined by a 12 inch filament wound sleeve. The joint was tested under hydrostatic pressure and failed at the edge of the joint near 1000 psi. Since the joint is the controlling factor for pipeline integrity, redesign is necessary so that burst pressures of the joint exceed burst pressures of the pipe specimens themselves. **Error! Reference source not found.** below shows a filament wound sleeve joint, which was produced by Kenway Corporation.



Figure 2-4: Filament Wound Sleeve Joint

The second type of joint under consideration is known as a heat fusion joint. The idea for this joint by was suggested by research being done at the Savannah River National Laboratory (non-proprietary). Heat fusion jointing is a welding process for the joining of polyethylene pipe. In this process, two pieces of pipe are heated at the same time and pressed together. As the pipes cool, the curing process forms a permeant bond. (Rawls 2014). At this point, very little work has been done to evaluate this joint. Once again, design and testing of this joint will take place during the second half of phase 2 of the project. **Error! Reference source not found.** shows the joint with liners, fillers, and mechanical connectors.

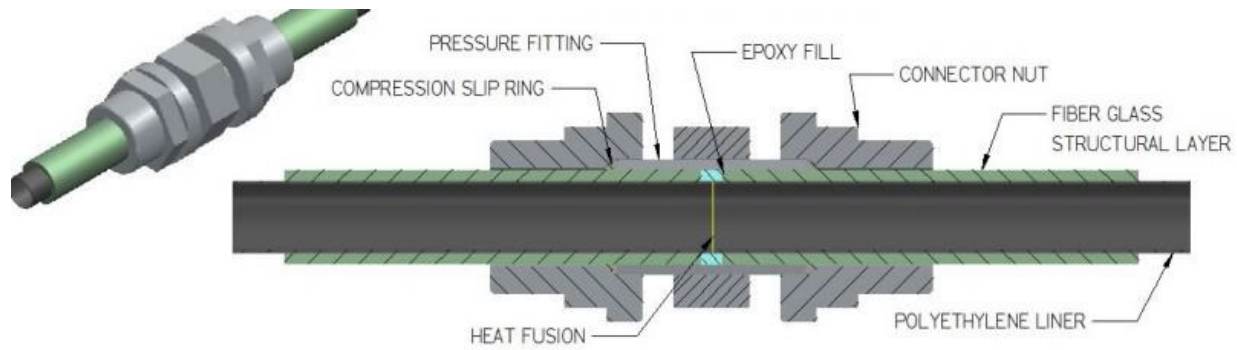


Figure 2-5: Heat Fusion Joint

2.4 Testing of Pipes

Pressure testing of pipes and joints have been conducted to achieve the goals of both phase 1 and phase 2 of this project. While phase 1 primarily focuses on detection of pipes, with a small focus on pressure testing, phase 2 is primarily focused on the evaluation of GFRP and CFRP pipes under high pressures. Phase 2 also focuses on the design and characterization of these pipes in accordance with ASME, ASTM, and API standards. At this point, three different categories of pressure tests have been conducted; pultruded pipe tests, pultruded pile tests, and filament wound pipe tests.

2.4.1 Pultruded Pipe Tests

The first pressure test conducted took place in the Fall of 2016. The test specimen was an orange, 24" long pultruded pipe with a 6" outer diameter and a wall thickness of 1/4" inch. This test was primarily intended as a preliminary test. The pipe specimen, which was manufactured by Creative Pultrusion, was already on hand and was of appropriate size for a low pressure test. One key issue associated with pressure testing of FRP pipes pertains to the endcaps. Most steel pipes simply have endcaps welded on, however, it is not possible to weld or bond FRP endcaps to FRP pipes, at least not in a way that can resist several hundred thousand pounds of resultant force. Therefore, the project team decided to utilize steel endcaps and an external load resisting system. **Error! Reference source not found.** shows this load system configured for the pultruded pipe.

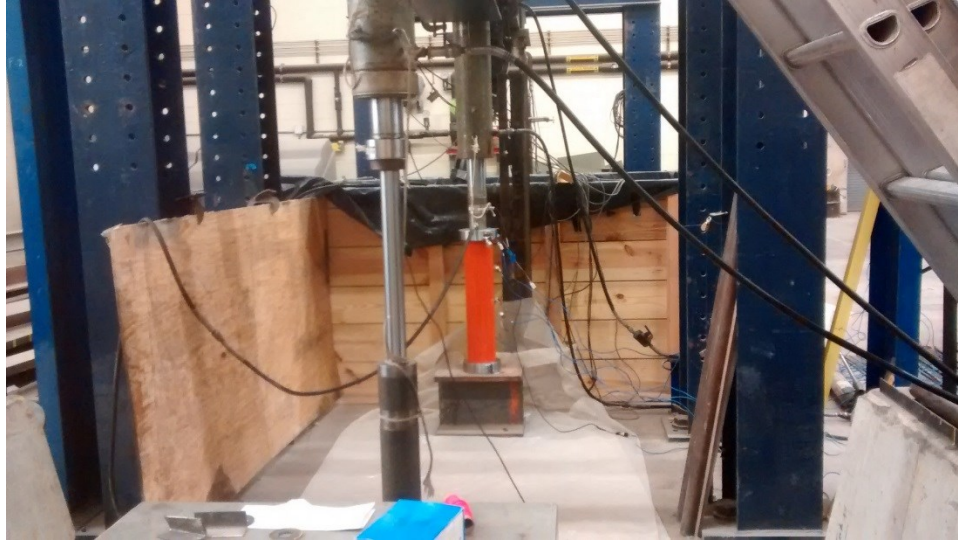


Figure 2-6: Load Resisting System

The test system is comprised of two main components, a pressure cylinder and the pressurized pipe. Load is applied, through an actuator, to a steel rod which compresses a small amount of water, seen in the foreground of **Error! Reference source not found..** As the pressure cylinder is loaded, the pressure flows through small hydraulic lines into the endcap of the pipe, seen in the background of **Error! Reference source not found..** An actuator above the pipe presses down on the endcap and prevents it from advancing off the end of the pipe. This pipe failed under 1000 psi in an unzipping fashion, breaking down the length of the pipe. This test allowed the project team to conclude that the test method adopted was acceptable.

2.4.2 Pultruded Pile Tests

The second set of tests was conducted in Spring of 2017. The specimens for this test were 36 inch long piles with outer diameter of 10 inches and a thickness of 3/8 inches. While piles, are very poorly suited for pressure applications, the team wanted to test the system for larger diameter pipe which would resist higher resultant loads. The same test methodology was used as stated earlier. These pipes failed either by unzipping along the pipe length or by expanding to the point that water began to seep through the walls (weeping). **Error! Reference source not found.** shows the pultruded pile fitted with the 10 inch diameter end caps.



Figure 2-7: Pultruded Pile

These piles failed under pressures near 300 psi. While these values are very low, the result was expected because piles have very little reinforcement in the hoop direction. Once again, the test methodology was found to be successful. However, the team did make a very important observation. During testing, eccentricities in the load frame resulted in the endcap rotation. This eccentricity was caused during the test preparation. If the center of the pipe (the center of pressure) was not placed directly under the center of the actuator (center of resistance), even by a fraction of an inch, the high resultant force combined with the small moment arm would cause the system to bend. This meant that the end cap was not restrained sufficiently by the relatively small diameter actuator. When the endcaps were poorly restrained, the rotation would cause the piles to leak before reaching any sort of failure. The cap would be forced onto one side, leading to crushing of the composite, while being lifted from the other side. To address this issue, the load frame was lowered and the actuator was shortened, thereby reducing the eccentricities and increasing the area of resistance. **Error! Reference source not found.** shows the eccentricity of the actuator and the endcap rotation.

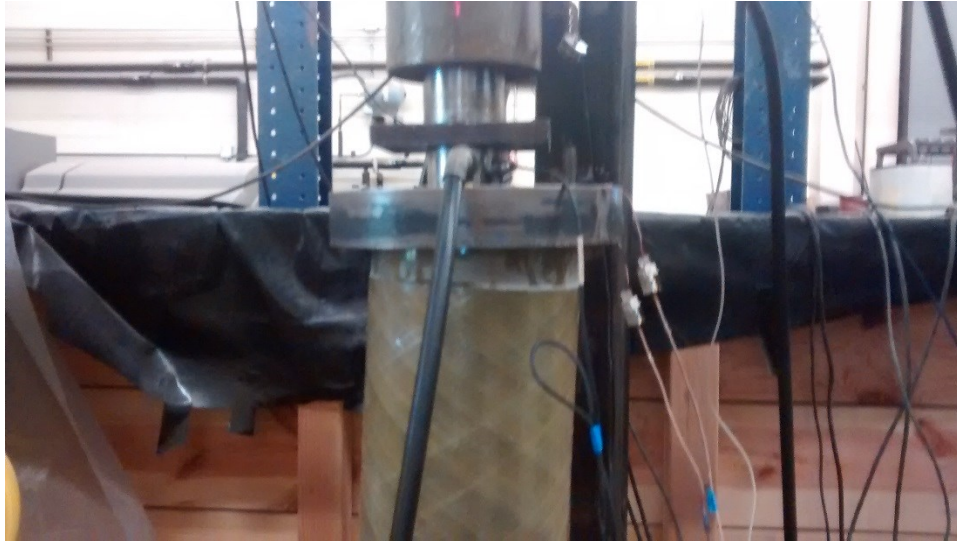


Figure 2-8: Eccentricity and Endcap Rotation

2.4.3 Filament Wound Pipe Tests

The third set of tests was conducted took place in April Spring of 2017. These specimens were 36 inch long, filament wound pipes, with a 10 inch outer diameter and a thickness of $\frac{1}{4}$ inch. These pipes were provided by Kenway Corporation. **Error! Reference source not found.** shows the filament wound pipe in the modified load frame. As can be seen, the frame is much lower to the ground and a much thicker actuator has been used. The combination of these two adjustments allowed the pipe to reach much higher internal pressures before leaking.



Figure 2-9: Filament Wound Pipe

These pipes were tested several times and have yet to fail, although the tests have been ended several times either due to premature leakage at the endcaps or due to limitations in the load frame. At this point, the pipes have withstood pressures up to 2300 psi, without failure. Due to limitations in the frame, a new load frame has been designed and is under fabrication. The project team hopes to proceed with testing during Fall of 2017 as a part of another USDOT-PHMSA funded project (Gangarao et al. 2016).

2.5 Conclusions

While the use of FRP pipe in pipelines does appear to have definite merit, there is significant work to be done if these sort of pipes are actually to be implemented on mass scale in pipelines. While the pipes have withstood pressures near 2300 psi, testing must demonstrate burst pressures of roughly 4 times this value (10,000 psi) before field application becomes reasonable. Furthermore, the joints must demonstrate burst pressures nearing 20,000 psi, since joints must be twice as strong as the pipes. Burst pressures in these ranges would allow composite pipelines to operate at pressures near 2000 psi, which would be about twice as high as the steel pipelines currently in operation. Research work on developing pipes capable of withstanding high burst pressures continues as a part of another USDOT-PHMSA funded project (Gangarao et al. 2016).

3 PIPE SET UP FOR GPR TESTING

3.1 Introduction

In order to determine the detectability of different pipeline materials buried at various depths using Ground Penetrating Radar (GPR), 33 pipe samples with different external surface configurations were prepared and buried in the field. Pipeline materials investigated in this research include Polyvinyl Chloride (PVC), Glass Fiber Reinforced Polymer (GFRP), and Carbon Fiber Reinforced Polymer (CFRP). The pipeline samples were all 5 ft. long, capped at both ends to prevent ground water from filling them when buried. The pipe sample preparation and experimental setup for the GPR testing is elaborated below.

3.2 Pipe Preparation

This research involved investigating the detectability of buried 12", 6", and 3" diameter PVC, GFRP, and CFRP pipes with different external surface finishes using GPR. Sample preparations of the various pipes are discussed below.

3.2.1 PVC pipes

The 12" diameter PVC pipes for testing were obtained by cutting 14 ft. long SDR-35 pipes into 5 ft. long segments. The pipes were then capped to prevent ground water from filling them after burying since the objective was to establish the pipe detectability without the help of GPR reflections from any water inside the pipes. Finally, the surfaces of two of the pipes were sanded to enable adequate bonding with CFRP fabric wrap as will be discussed later in this chapter. The 12" diameter PVC pipes are shown in Figure 3-1.

Similar to the 12" diameter PVC pipes, 14 ft. long SDR-35 and 10 ft. long schedule 40 (SCH 40) pipes were cut to obtain the 5 ft. long 6" and 3" diameter pipe samples respectively. The 6" and 3" diameter pipes were also capped, and the surfaces of some of them were grinded to enable adequate bonding with GFRP and CFRP fabric (Figure 3-2).

3.2.2 GFRP pipes

The 12" diameter GFRP pipes used in this study were supplied by the manufacturer in 5 ft. long segments (Figure 3-3). The pipes were capped to keep ground water out of the pipes after burying. The external surface of some of the pipes were sanded to ensure adequate bonding with CFRP fabric wrap.

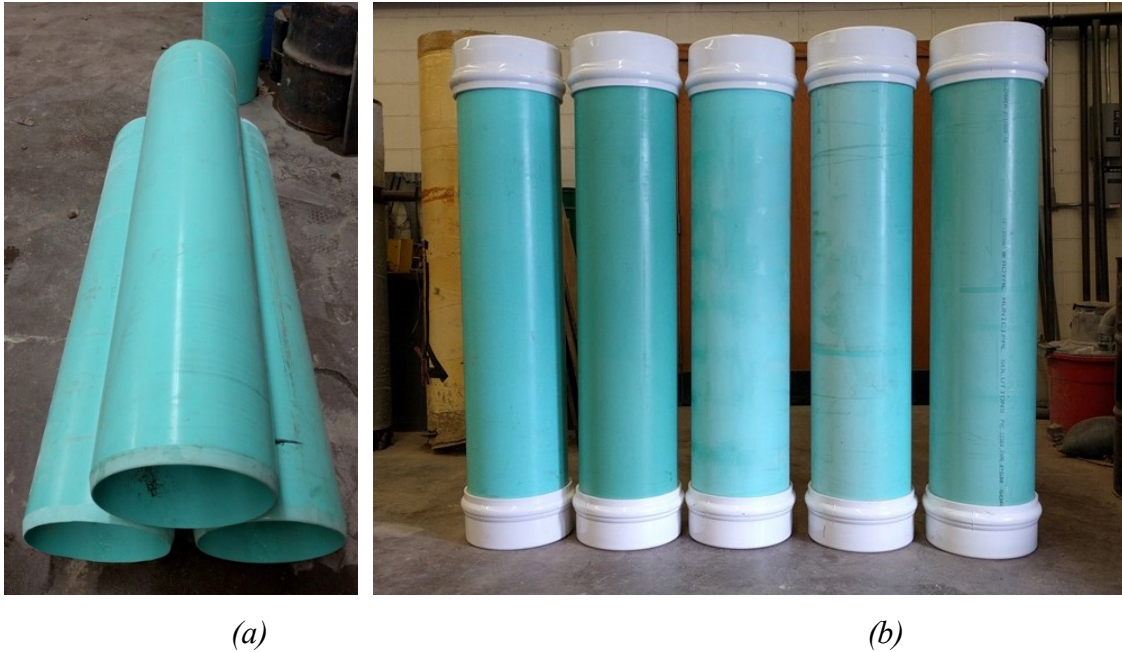


Figure 3-1: The 12" diameter PVC pipe (a) after cutting, and (b) after capping



Figure 3-2: The 3" diameter PVC pipes

The 3" diameter GFRP pipes for the study were manufactured in the WVU Constructed Facilities Center (CFC) by wrapping two layers of 24 oz. biaxial (0/90) stitched GFRP fabric around 3" diameter PVC pipes (the PVC pipes serving as molds in this process). This increased the outside diameter of the GFRP pipes above the standard 3" PVC pipe dimension. Details of the GFRP fabric and the resin (matrix) system used in manufacturing the 3" GFRP pipe is shown in Table 3-1. The manufacturing process and a completed GFRP pipe are illustrated in Figure 3-4.



(a) GFRP pipes from the manufacturer

(b) Capped pipes

Figure 3-3: The 12" diameter GFRP pipes

Table 3-1: Material and section properties of CFRP and GFRP pipes/fabrics used

Pipe Section	Wall Thickness (in)	Fiber Material	Fiber Mat	Fiber Weight (oz. /sq. yd.)	Matrix Material
12" GFRP	3/8	E-Glass	45/90/-45	-	Polyurethane
3" GFRP	**	E-Glass	0/90	24	Vinyl Ester
12" CFRP	**	Carbon	0/90/±45	28	Vinyl Ester
CFRP Strip/Ring	*	Carbon	0/90/±45	28	Vinyl Ester
3" CFRP	5/16	Carbon	-	-	-

* One layer of fabric was used.

** Two layers of fabric were used.

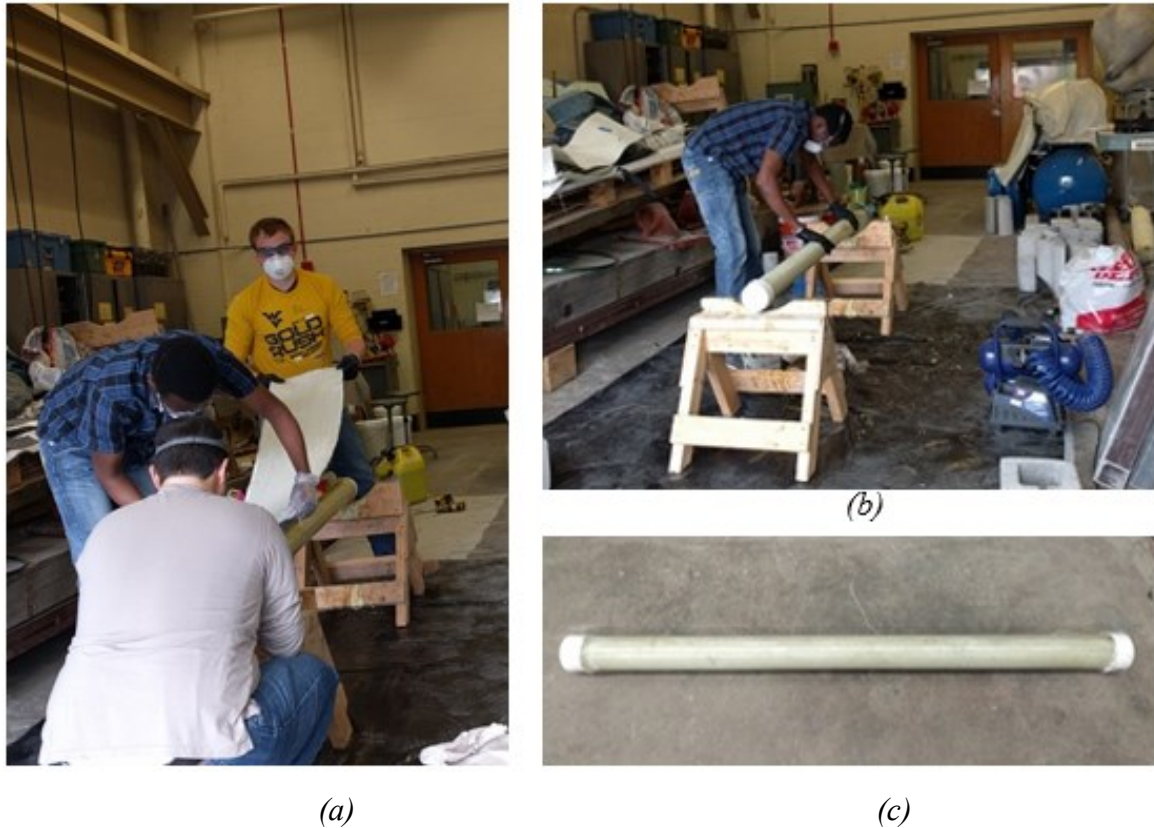


Figure 3-4: 3" diameter GFRP pipes (a), (b) manufacturing process, and (c) a completed pipe

3.2.3 CFRP pipes

The 12" diameter CFRP pipe used in this study was also fabricated in the WVU Constructed Facilities Center (CFC) by wrapping two layers of quad-axial (0/90/±45) stitched CFRP fabric around a 12" diameter cardboard tube (the cardboard tube served as a mold in this process). Details of the CFRP fabric and the resin system used in manufacturing the 12" CFRP pipe is shown in Table 3-1. The pipe was finally capped to keep ground water out of it after burying. Figures 3-5(a) and 3-5(b) show the CFRP fabric and the completed 12" diameter CFRP pipe respectively

The 3" diameter CFRP pipes used in this study were supplied by the manufacturer in 6 ft. long segments (Figure 3-6). The pipes were first cut into 5 ft. long segments to keep the lengths consistent with the other pipes, they were then capped to keep ground water out of them after burying.



(a) Roll of CFRP fabric



(b) The completed pipe

Figure 3-5: 12" diameter CFRP pipe



Figure 3-6: The 3" diameter CFRP pipes

3.2.4 Using CFRP fabric and aluminum foil tape to make non-metallic pipes detectable

Non-metallic pipe materials (such as PVC and GFRP) buried underground are generally not detectable using GPR in most soil conditions. This is because PVC and GFRP pipe materials have similar dielectric constant as most soils. In order to make these pipe materials detectable after burying using GPR, we have to create a contrast between the dielectric constants of the pipes and the surrounding soil. Two different approaches were adopted to create dielectric contrast between

the pipe materials and the sounding soil - using CFRP rings and strips, and using aluminum rings and strips.

Carbon fiber and aluminum tape, like steel, are electrical conductors and as such do not allow transmission of radio waves like GPR signal. GPR signal incident on carbon fiber/aluminum material is reflected back to a receiver (unlike the surrounding soil, which absorbs and/or allows the signal to travel through), thereby making the material detectable underground.

Some of the PVC and GFRP pipes were wrapped with CFRP fabric and aluminum tapes, in the form of rings and strips to improve GPR detectability of these pipes. The carbon fabric and aluminum rings are 3" wide, and placed at 3" clear spacing while the carbon fabric strip and aluminum strips covered half of the pipe circumference and stretched the full length of the pipes (excluding pipe caps in most cases). Some of the wrapped pipes are shown in Figure 3-7. Some of the PVC and GFRP pipes were not wrapped (these are labelled as "Unwrapped" in Figure 3-9), and were used as control specimens during GPR detectability testing of the samples.

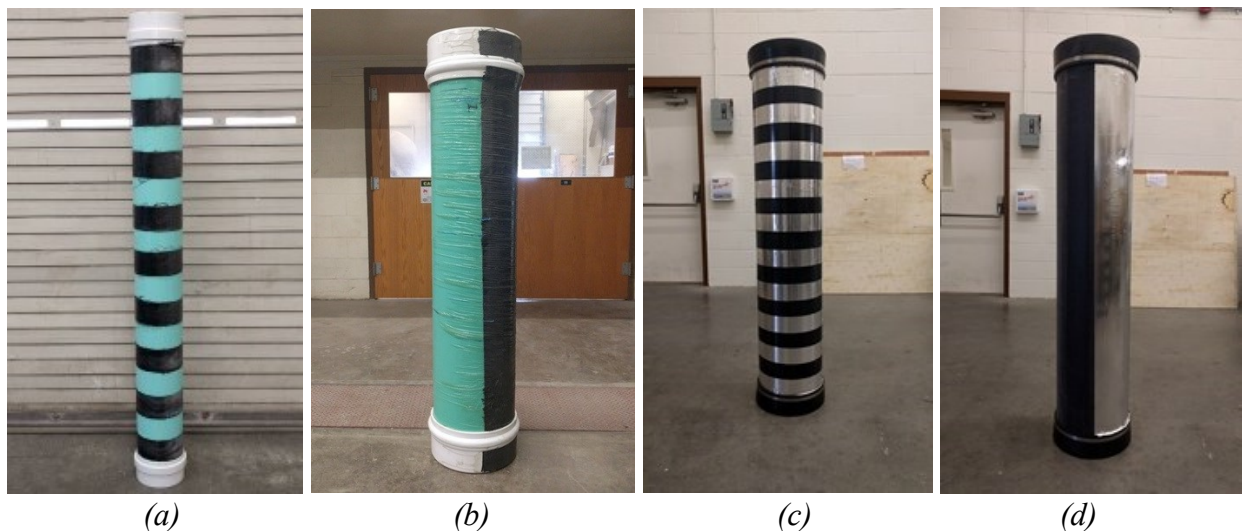


Figure 3-7: Completed (wrapped) pipes: (a) 6" diameter PVC with carbon fabric rings, (b) 12" diameter PVC with carbon fabric strip, (c) 12" diameter GFRP with aluminum rings, and (d) 12" diameter GFRP with aluminum strip

A total of 33, 5 ft. long pipe segments were prepared using different pipe materials (CFRP, GFRP, and PVC), different pipe diameters (12", 6", and 3"), different surface finishes (CFRP ring, CFRP strip, aluminum ring, aluminum strip, and unwrapped/control), and buried at different depths (2 ft., 3 ft., and 4 ft. of soil cover above the top of the pipe).

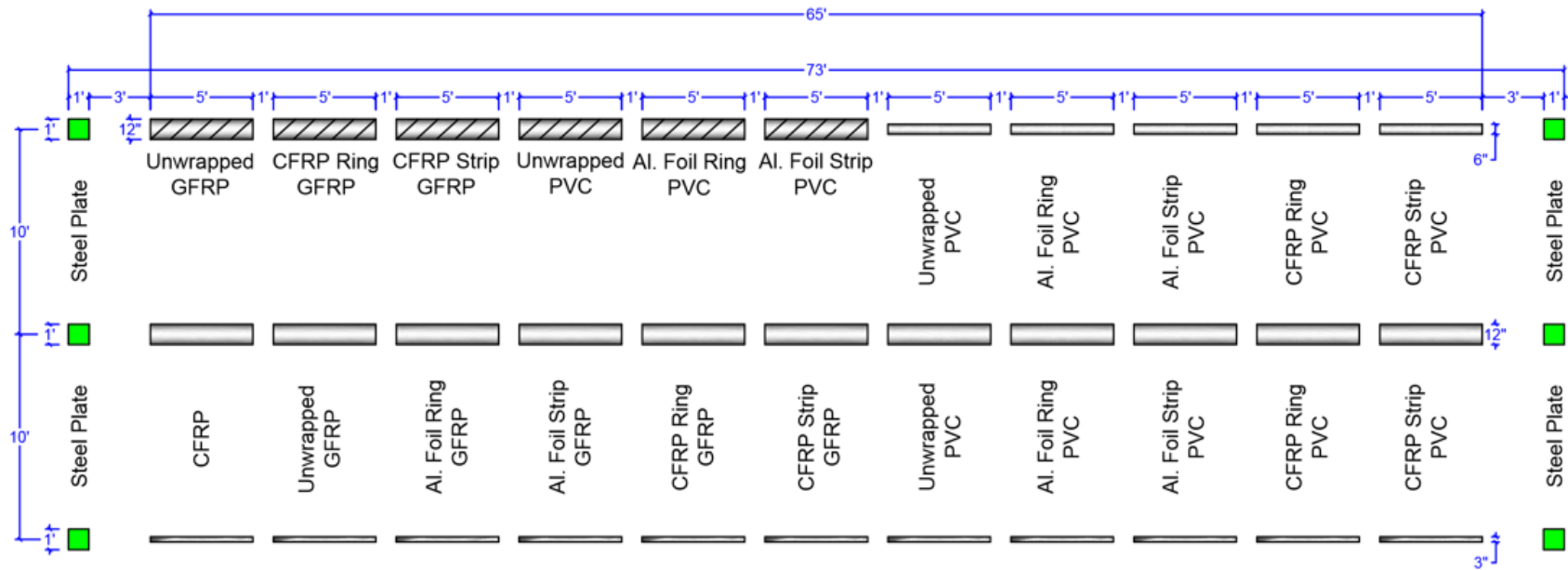
3.3 Pipe Burying

Pipe specimens prepared for GPR testing were buried at a site located on the WVU campus. Utility lines close to the allocated site were first marked to prevent excavation damage of the lines during pipe burying. The site and the marked utility lines are shown in Figure 3-8.

The pipe samples were buried in 3 separate 65 ft. long trenches, spaced at 10 ft. apart. 12" diameter and 5 ft. long PVC, CFRP, and GFRP pipes were buried at a depth of 4 ft. in one of the trenches (total trench depth of 5 ft.). The second trench had 3" diameter pipes buried at a depth of 2 ft. (total trench depth of 27"). Two different diameter pipes, 12" and 6", were buried in the third trench, both diameters buried at a depth of 3 ft. to the top of the pipe. Eleven pipes were buried in each trench, with 1 ft. spacing between each subsequent pipe as shown in Figure 3-9 and 3-10(a). The layout of the pipes, including the pipe material, diameter, pipe surface configuration and depth of burial are shown in Figure 3-9. Additionally, 5 GS3 soil sensors (Figure 3-10(b)) were buried along the trenches at different depths to measure soil properties throughout the testing period. Two of the sensors were buried at 4 ft. depth along the 12" diameter pipes, two were buried at 2 ft. depth along the 3" diameter pipes and one was used to measure soil properties at various locations on the ground surface. Wires connecting the soil sensors to a data logger were run through 1" diameter PVC conduits before burying to prevent the wires from getting damaged during compaction of backfill. These sensors enabled quantitative determination of volumetric water content, electrical conductivity, temperature, and dielectric constant of the soil during the testing period.



Figure 3-8: The located site within WVU campus for burying the pipes








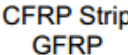
-  Steel plates buried at a depth of 3"
-  12" diameter pipes buried at a depth of 48" (Total trench depth of 60")
-  12" diameter pipes buried at a depth of 36" (Total trench depth of 48")
-  6" diameter pipes buried at a depth of 36" (Total trench depth of 42")
-  3" diameter pipes buried at a depth of 24" (Total trench depth of 27")
-  CFRP Strip GFRP GFRP pipe with CFRP fabric strip over half of the pipe circumference. Similar naming scheme applies to the other pipes in the layout

Figure 3-9: Pipe layout for GPR testing



Figure 3-10: (a) Arrangement of pipes in the trench, (b) soil moisture and resistivity sensor

Figure 3-11(a and b) show the 12" and 6" diameter pipes placed at 3 ft. depth (to the top of the pipe) in the trench and the pipes being covered with backfill. Figure 3-11(c) shows some of the 12" diameter pipes placed in the trench at 4 ft. depth (to the top of the pipe). Two 1 ft. wide steel plates were buried at 3" depth (one at each end of the trench) to mark the beginning and end of each trench for GPR testing.

Finally, the trenches were backfilled, the ground surface was levelled and then seeded with grass (Figure 3-12) to restore the initial field condition before GPR testing.

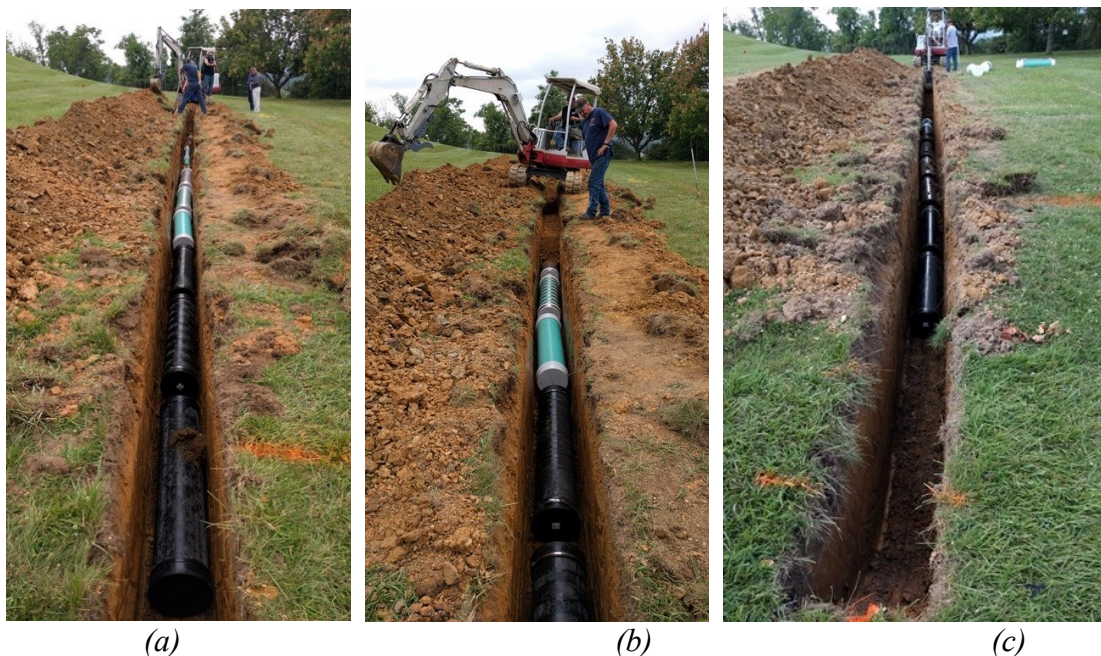


Figure 3-11: 12" and 6" diameter pipes being buried



Figure 3-12: (a) The site being seeded, (b) the field restored to initial condition

Multiple GPR tests were conducted after the grass had grown to the initial condition. The GPR test results are discussed in the next chapter.

3.4 Conclusions

This chapter summarized the sample preparation and material properties of the pipe specimens used in the GPR detectability testing. The following chapter presents and discusses the GPR test results.

4 GPR TESTS AND RESULTS

4.1 Introduction

Different pipe material samples (CFRP, GFRP, and PVC) with different external surface finishes were buried at a test site as explained in Chapter 3. GPR tests were conducted under different soil moisture conditions (indicated by the changing soil dielectric constant for each test), and using different antennae frequencies (200 MHz and 400 MHz). The results of these tests are presented in the following sections.

4.2 GPR Equipment

The GPR system used in this study was the SIR-20 model manufactured by Geophysical Survey Systems, Inc (GSSI). A 200 MHz antenna with a specified penetration depth of up to 30 ft. (in dry sand) and a 400 MHz antenna with a specified penetration depth of up to 12 ft. (in dry sand) were evaluated with this system. The quoted penetration depths depends on the complex dielectric permittivity of the soil medium, and therefore can be significantly lower in soils with high moisture contents and high clay content. The GPR system and antennae used in this study are shown in Figure 4-1.

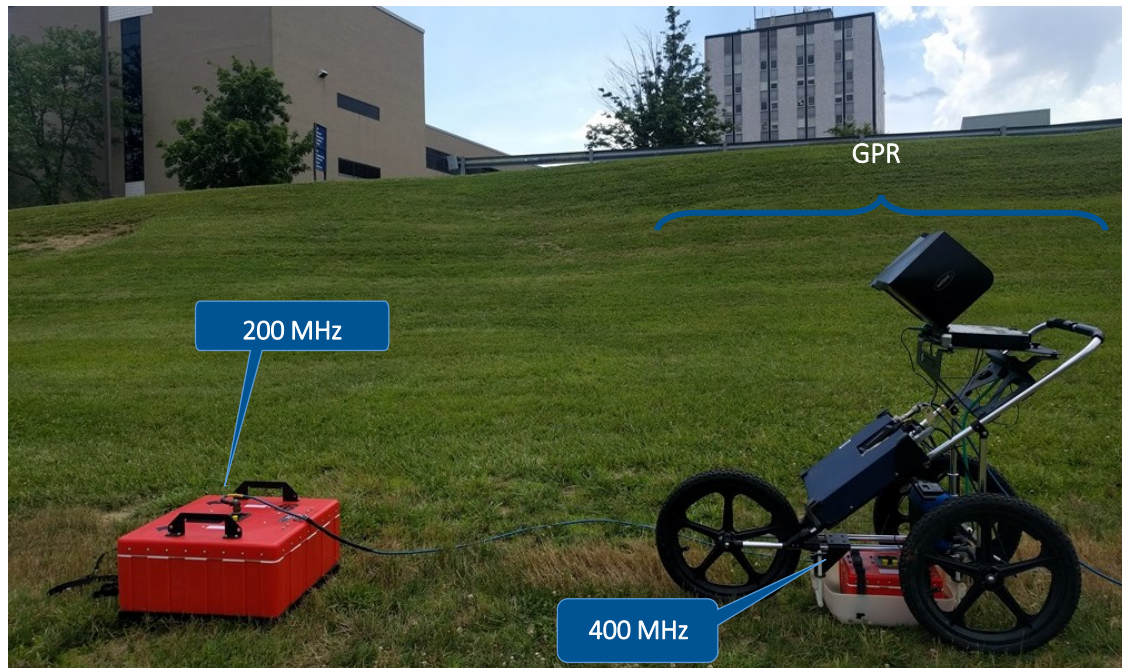


Figure 4-1: SIR-20 GPR system and antennae used for testing

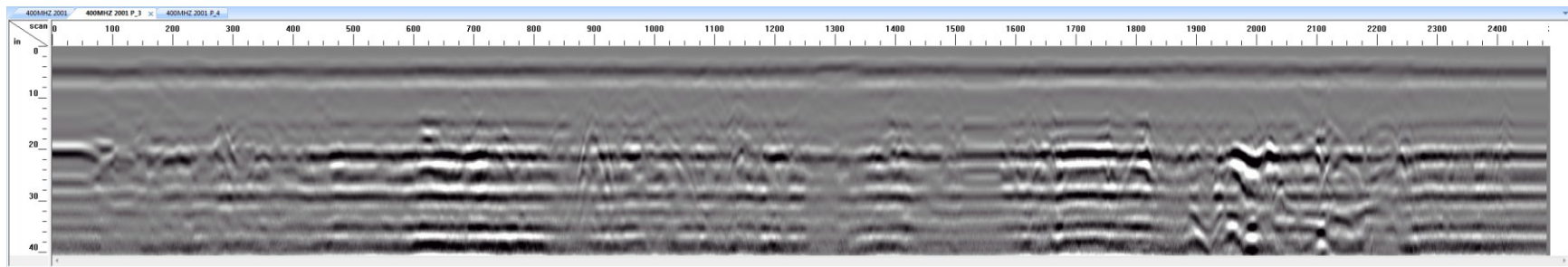
The GPR system has survey wheels with optical encoder for tracking horizontal distance along the ground surface. A survey wheel attached to the GPR cart is used to track distance when the 400 MHz antenna is used, while the 200 MHz antenna has a survey wheel attached to the antenna for horizontal distance measurement as shown in Figure 4-2.



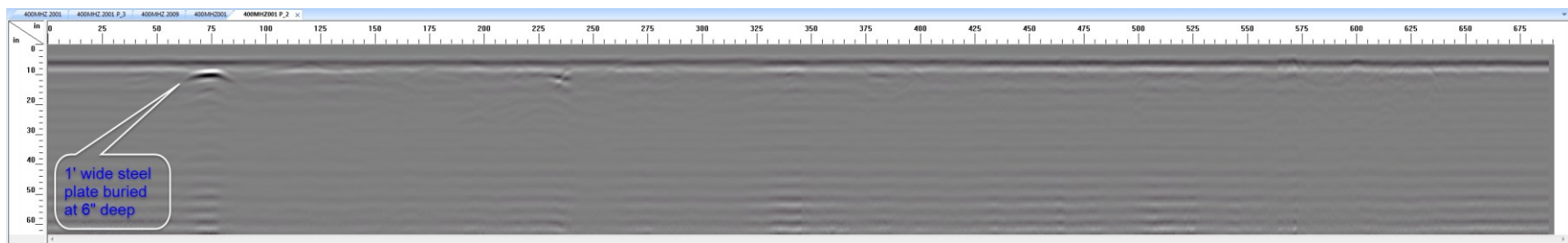
Figure 4-2: 200 MHz GPR antenna with survey wheel

4.3 GPR Test Results

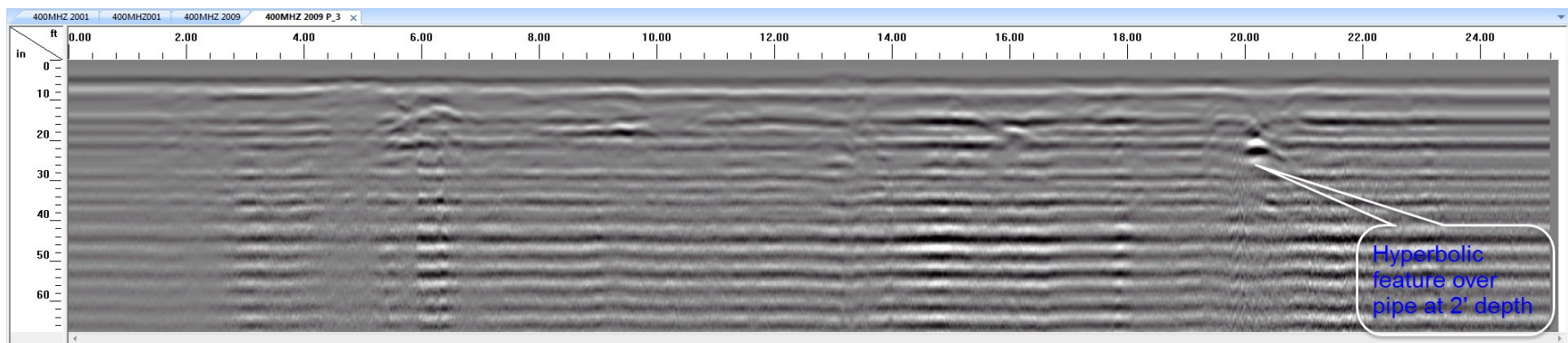
Multiple GPR scans were carried out in both the longitudinal direction along the trenches, and transverse direction across the pipe/trenches. All the trenches were scanned with both the 200 MHz and 400 MHz antennae, and some of the data obtained are shown in the following figures (Figures 4-3 through 4-22). Figures 4-3 and 4-4 show some of the data from longitudinal and transvers scans over the trenches using a 400 MHz antenna (this data is named “Dataset I”). Average soil dielectric constant for the data in Figures 4-3 and 4-4 were 19.75 and 21.65 for up to a depth of 2 ft. and 4 ft. respectively. Dielectric constants for this dataset, together with other datasets are summarized in Table 4-1. The 400 MHz antenna was able to locate most of the pipes located at 2 ft. depth. Signals from this antenna are particularly good over pipes with CFRP fabric wraps/overlays as shown in Figure 4-4 (a) and (b). The 400 MHz antenna was however not able to locate any of the pipes buried below 2 ft. of soil cover as can be seen from Figure 4-3(b) for 3 ft. of soil cover. The remainder of this chapter will focus on data obtained from the deeper penetrating 200 MHz antenna.



(a) Longitudinal scan along the full length of 3" diameter pipes with 2 ft. of soil cover

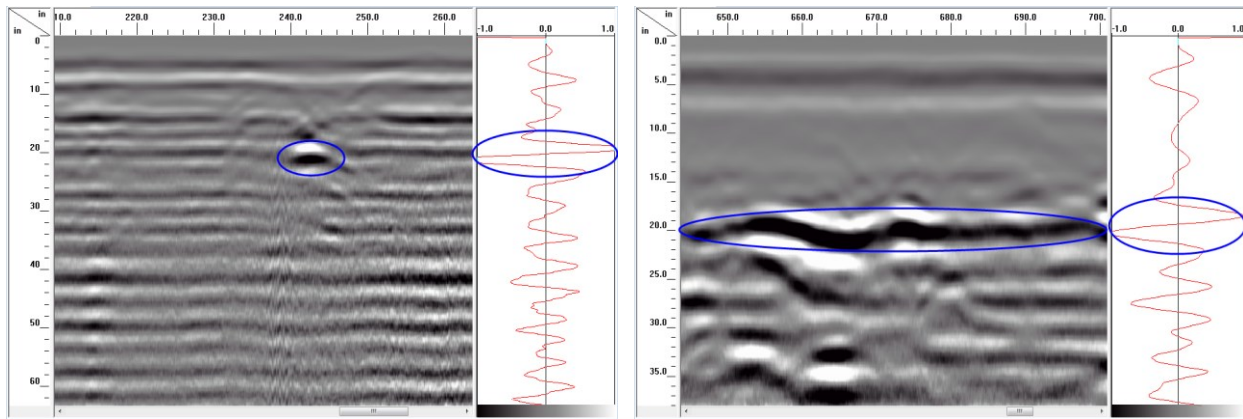


(b) Longitudinal scan along the full length of 12" and 6" diameter pipes with 3 ft. of soil cover

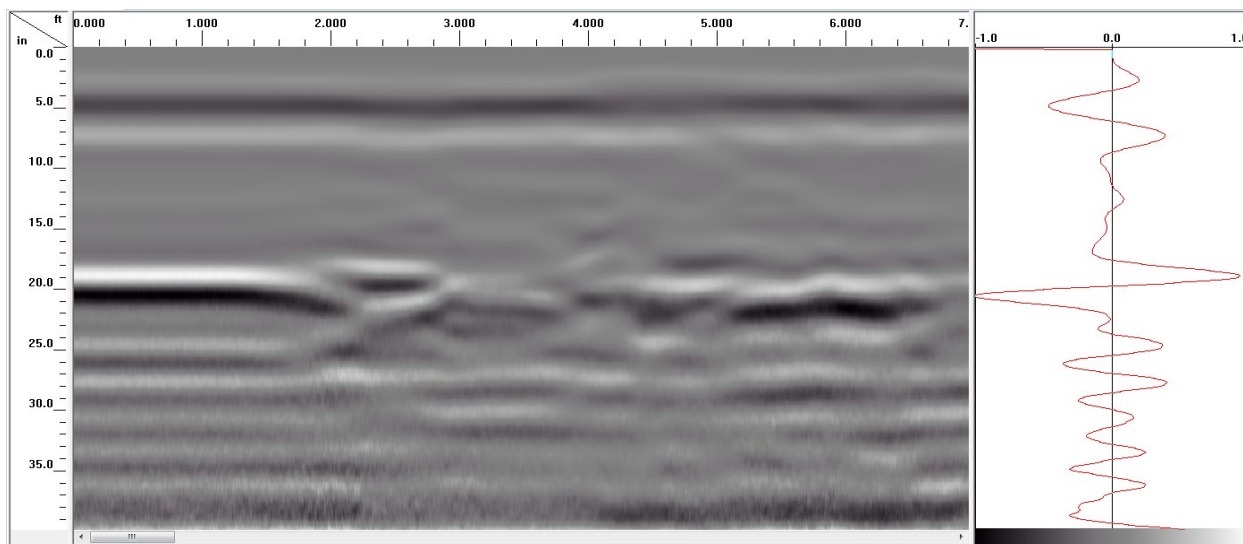


(c) Transverse scan across all the 3 trenches, from the 3 ft. deep to the 2 ft. deep one

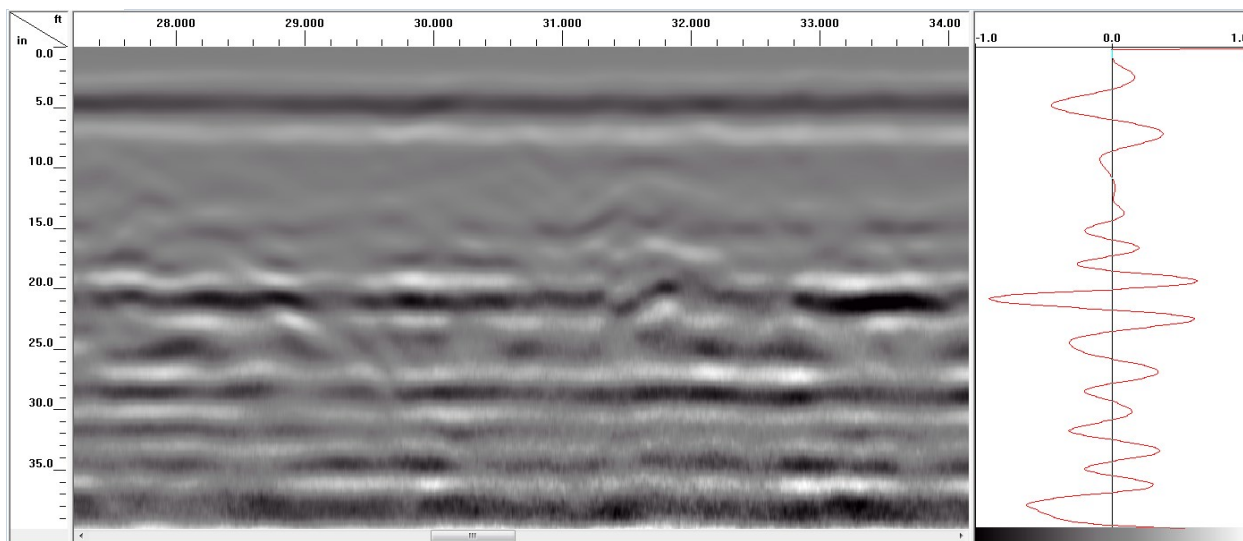
Figure 4-3: Longitudinal and transverse scans over the trenches using 400 MHz GPR antenna



(a) Transvers scan over pipe wrapped with CFRP (b) Longitudinal scan over the pipe in (a)



(c) Longitudinal scan over some of the 3" diameter pipes with 2 ft. of soil cover



(d) Longitudinal scan over some of the 3" diameter pipes with 2 ft. of soil cover

Figure 4-4: Close up views of scans over 3" diameter pipes using 400 MHz GPR antenna

The 200 MHz antenna produced a better result at deeper depths (more than 2 ft. depth), as well as a good result at 2 ft. depth. Two different GPR datasets (Dataset II and Dataset III) obtained using the 200 MHz antenna are presented and compared. Average dielectric constants of the soil up to the different depths at which pipes were buried (measured at the time of GPR testing) are provided in Table 4-1. Raw data from scans over the three trenches for Dataset II are shown in Figure 4-5 (a) through (c) for comparison. Figures 4-6 through 4-8 show the raw scans over the trenches compared to the processed scans from each trench. “Peaks extraction” data processing technique was used to obtain the processed data.

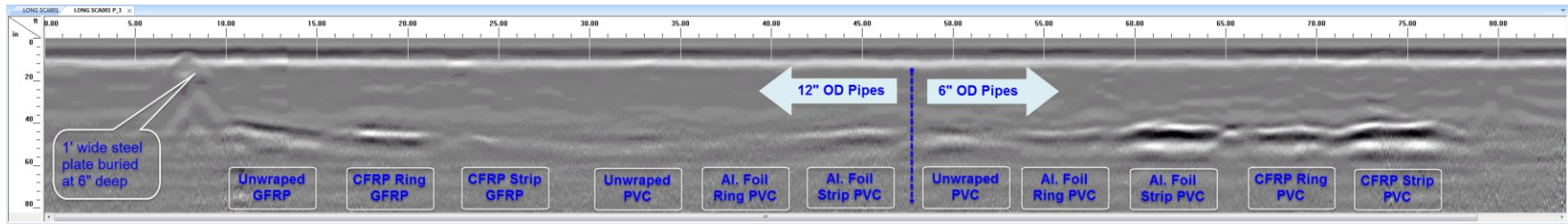
Table 4-1: Average soil dielectric constant during data collection

Up to Depth	Dataset I	Dataset II	Dataset III
2"	19.75	17.11	16.57
3"	20.70	18.52	17.93
4"	21.65	19.94	19.30

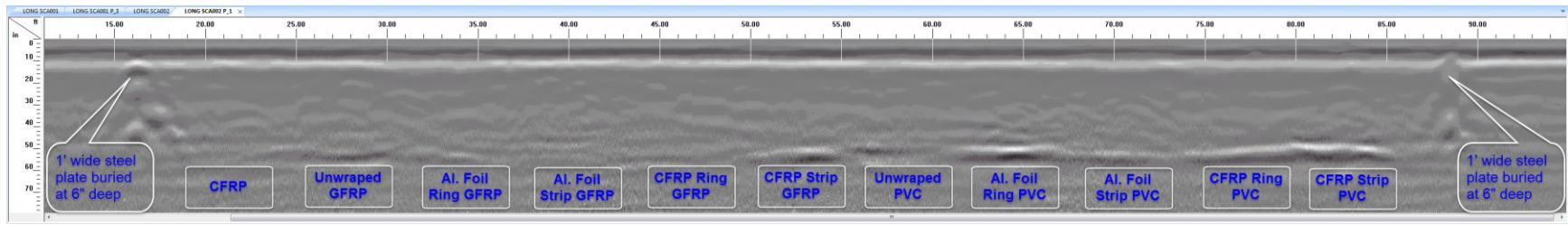
It is observed from Dataset II (Figures 4-5 through 4-8) that, aluminum foil and carbon fabric wraps/overlay on the pipe sections improve detectability with GPR. It is also observed that, aluminum strips and carbon fabric strips along the full length of the pipe sections produce better results compared to aluminum rings and carbon fabric rings.

Figures 4-9 through 4-11 show raw scan from Dataset III, together with the processed form of the same data for comparison. Visibility of pipe segments in the GPR scans from Dataset III are better than those from Dataset II. This can be due to the slightly lower soil dielectric constant and lower moisture content (lower signal attenuation) for Dataset III. By comparing results from the 3 ft. deep trench from the two datasets (Figures 4-6(b) and 4-9(b)), two pipe sections which were not visible in Dataset II (CFRP Strip GFRP and Al. Foil Ring PVC from the 12" OD Pipes side of the trench) can be seen in Dataset III. Also, the visibility of the Unwrapped PVCs are greatly improved in Dataset III.

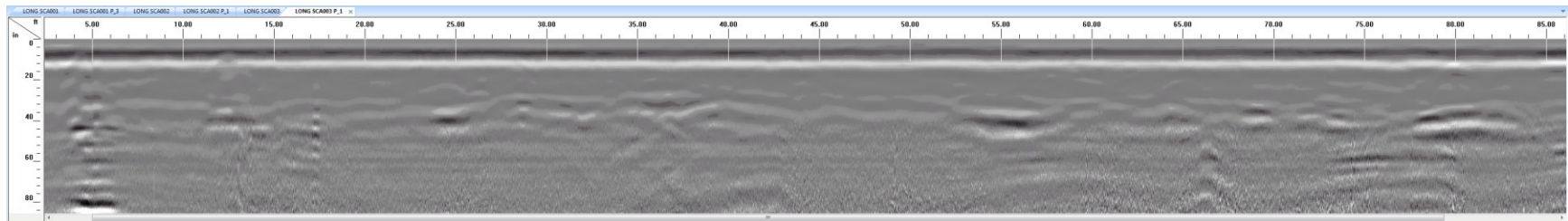
It can also be seen in Figures 4-7(b) and 4-10(b) – data from the 4 ft. deep trench – that the following pipe sections, CFRP, Al. Foil Ring GFRP, Al. Strip GFRP, and CFRP Ring GFRP, which were not visible in Dataset II are visible in Dataset III. The visibility of the other pipes in this 4 ft. deep trench has also been significantly improved in Dataset III.



(a) Longitudinal scan along the full length of 12" and 6" diameter pipes with 3 ft. of soil cover

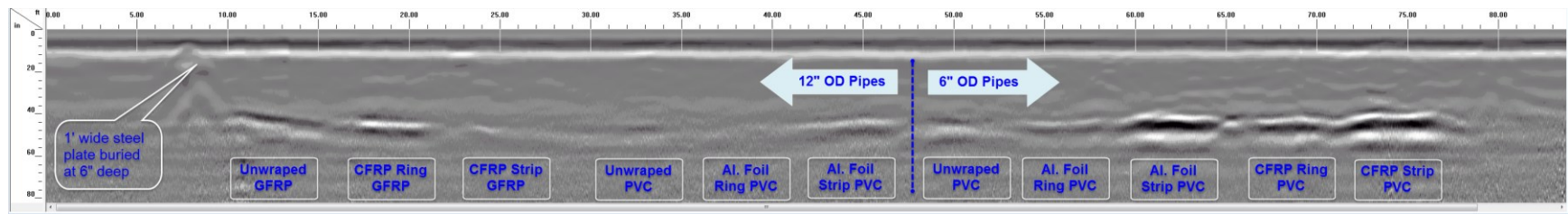


(b) Longitudinal scan along the full length of 12" diameter pipes with 4 ft. of soil cover

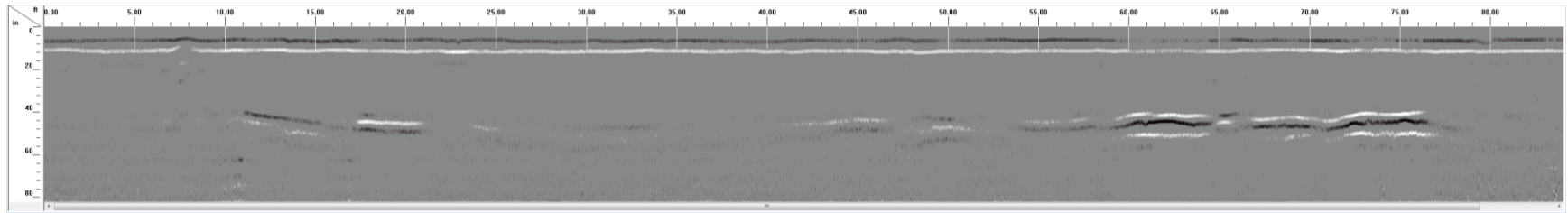


(c) Longitudinal scan along the full length of 3" diameter pipes with 2 ft. of soil cover

Figure 4-5: Dataset II - Longitudinal scans along the full length pipe trenches using 200 MHz GPR antenna

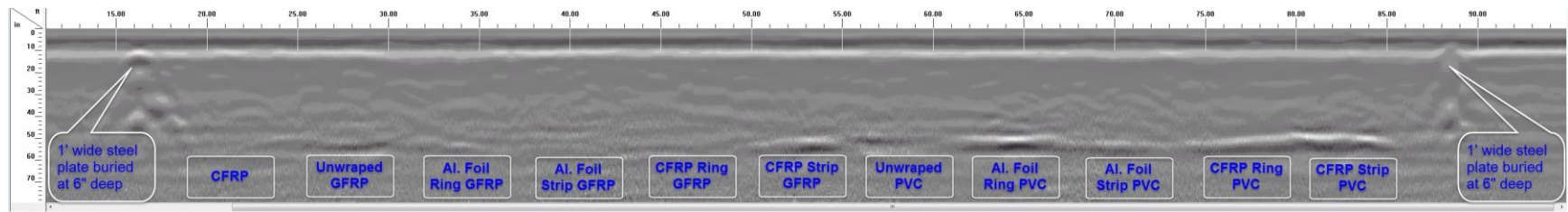


(a) Longitudinal scan along the full length of 12" and 6" diameter pipes with 3 ft. of soil cover

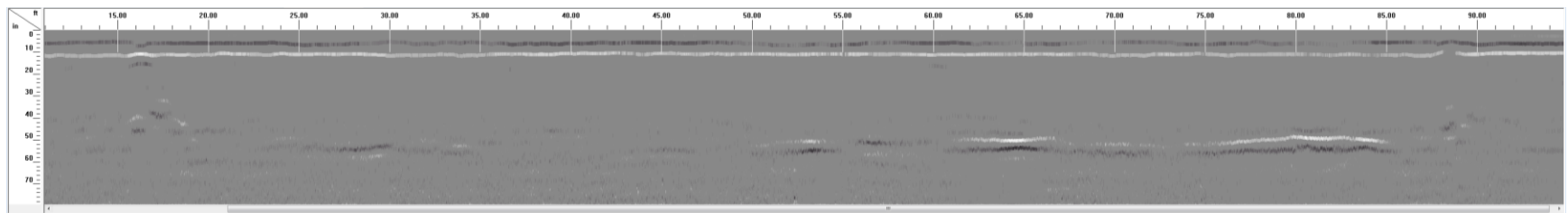


(b) Processed longitudinal scan using peak extraction to make pipe sections more visible

Figure 4-6: Dataset II - Longitudinal scan and the processed data along the full length of 3 ft. deep trench

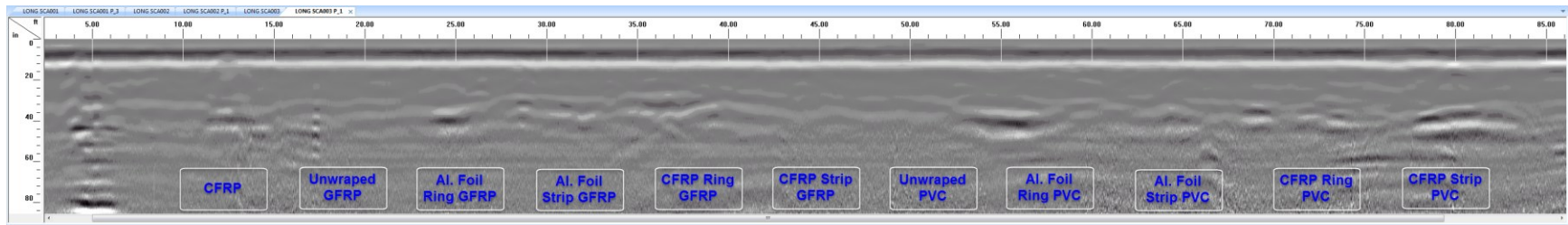


(a) Longitudinal scan along the full length of 12" diameter pipes with 4 ft. of soil cover

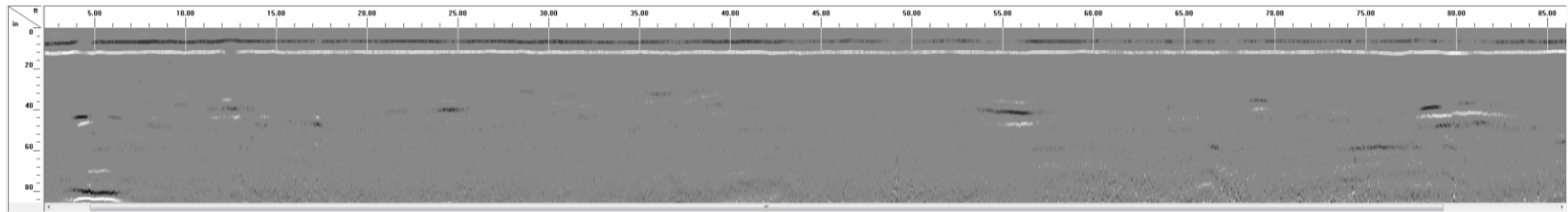


(b) Processed longitudinal scan using peak extraction to make pipe sections more visible

Figure 4-7: Dataset II - Longitudinal scan and the processed data along the full length of 4 ft. deep trench

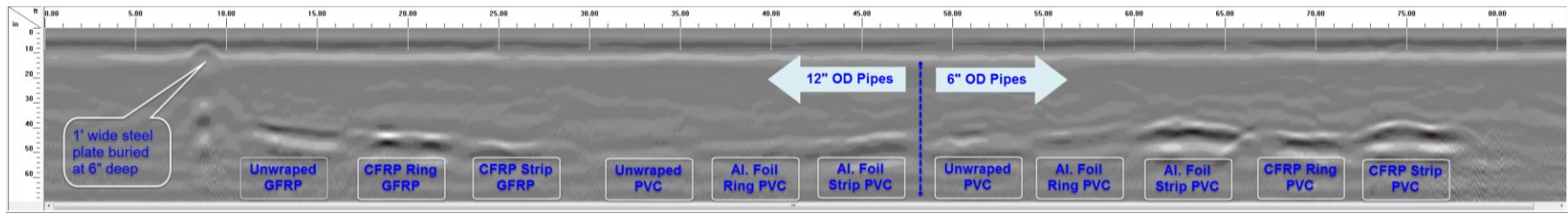


(c) Longitudinal scan along the full length of 3" diameter pipes with 2 ft. of soil cover

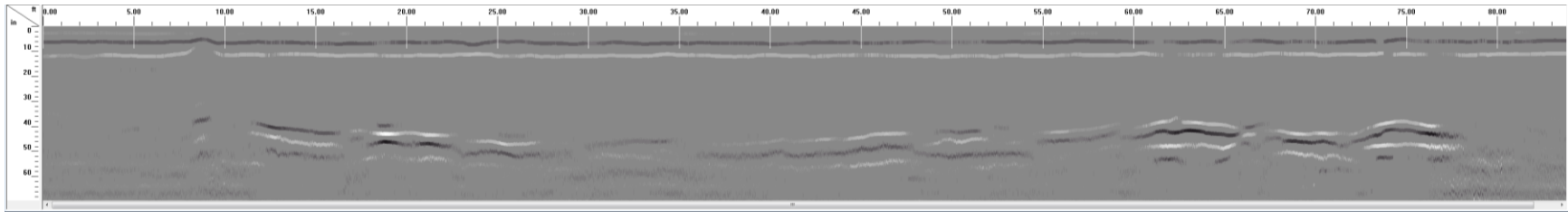


(b) Processed longitudinal scan using peak extraction to make pipe sections more visible

Figure 4-8: Dataset II - Longitudinal scan and the processed data along the full length of 2 ft. deep trench

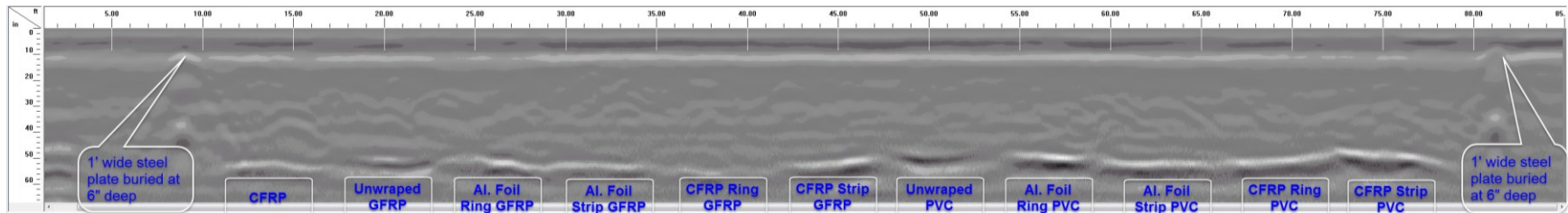


(a) Longitudinal scan along the full length of 12" and 6" diameter pipes with 3 ft. of soil cover

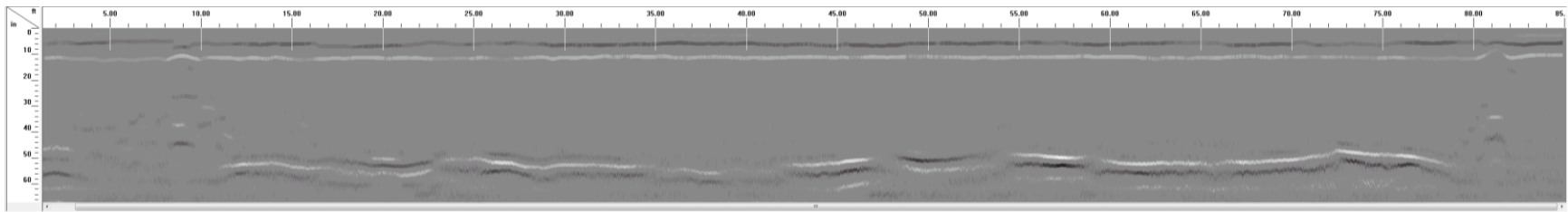


(b) Processed longitudinal scan using peak extraction to make pipe sections more visible

Figure 4-9: Dataset III - Longitudinal scan and the processed data along the full length of 3 ft. deep trench

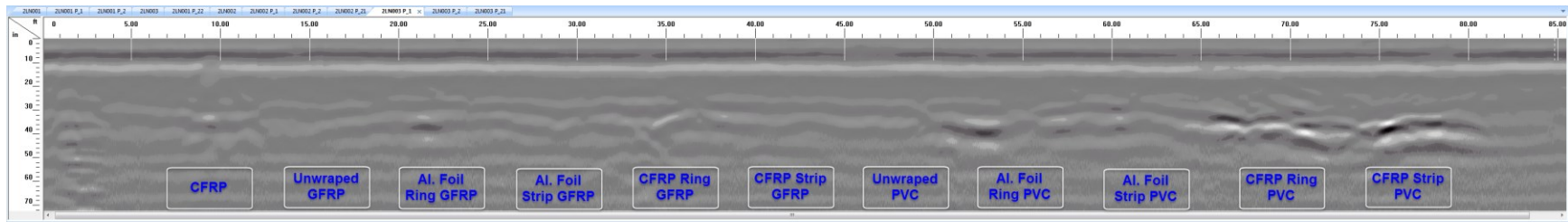


(a) Longitudinal scan along the full length of 12" diameter pipes with 4 ft. of soil cover

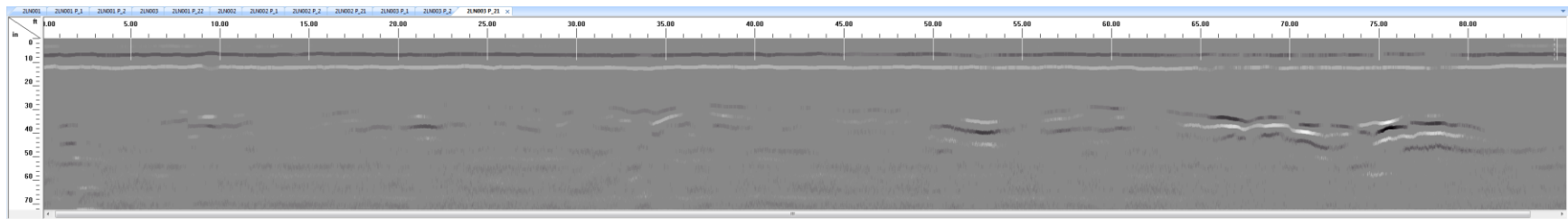


(b) Processed longitudinal scan using peak extraction to make pipe sections more visible

Figure 4-10: Dataset III - Longitudinal scan and the processed data along the full length of 4 ft. deep trench



(c) Longitudinal scan along the full length of 3" diameter pipes with 2 ft. of soil cover



(b) Processed longitudinal scan using peak extraction to make pipe sections more visible

Figure 4-11: Dataset III - Longitudinal scan and the processed data along the full length of 2 ft. deep trench

GFRP and PVC pipe sections with no carbon fabric or aluminum foil overlay (Unwrapped GFRP and Unwrapped PVC) were not visible in both Dataset II and III from the 2 ft. deep trench (Figures 4-8 and 4-11), which consisted of only small (3") diameter pipes. Other pipe sections which were not visible in Dataset II from this trench were visible in the processed data in Dataset III, though the signal is faint as shown in Figure 4-11(b). Finally, the visibility of the remaining pipe sections in this trench (the ones with aluminum or carbon fabric rings or strips) were improved in Dataset III compared to Dataset II.

The following figures (Figures 4-12 through 4-22) show the longitudinal scan or B-scan (left side of the figures) and A-scan (right side of the figures) over some of the pipe sections in Dataset III. Only scans from the 3 ft. deep trench are shown for brevity. Measurement of soil dielectric constant using buried soil sensors during GPR data collection enabled accurate determination of the depth at which pipe sections were buried, as shown in Figure 4-12, where the measured pipe depth of 35.87" using GPR A-scan signal correlates very well with the actual pipe depth of 36". It should also be noted from Figure 4-12 that the unwrapped 12" diameter GFRP pipe show up fairly well in the GPR scan at 3 ft. depth.

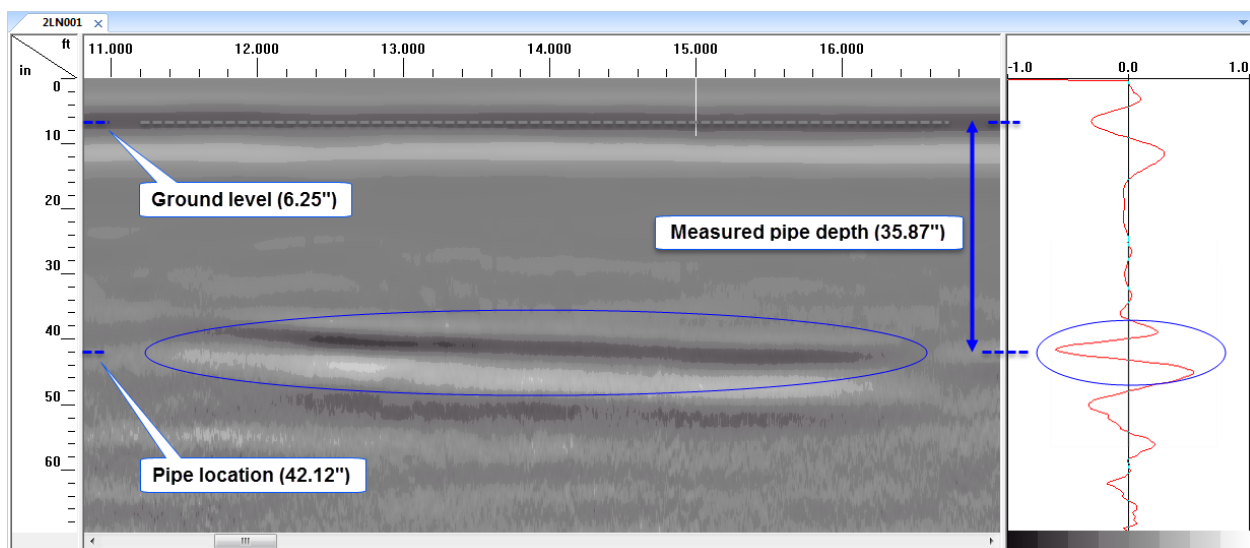


Figure 4-12: Longitudinal GPR scan (left) and A-Scan (right) over 12" Unwrapped GFRP pipe

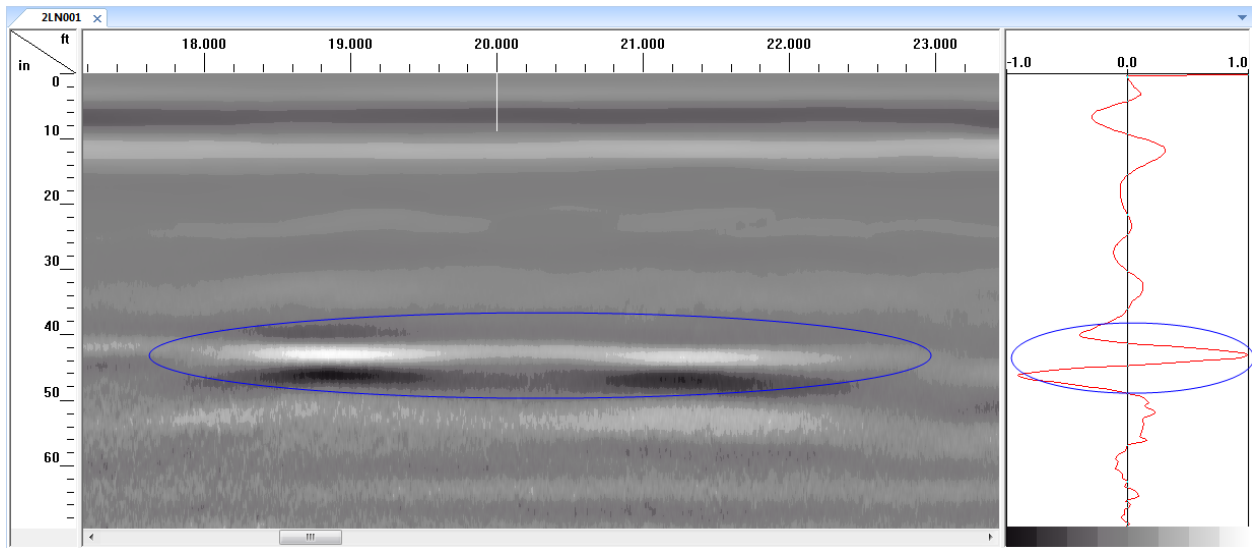


Figure 4-13: Longitudinal GPR scan (left) and A-Scan (right) over 12" CFRP Ring GFRP pipe

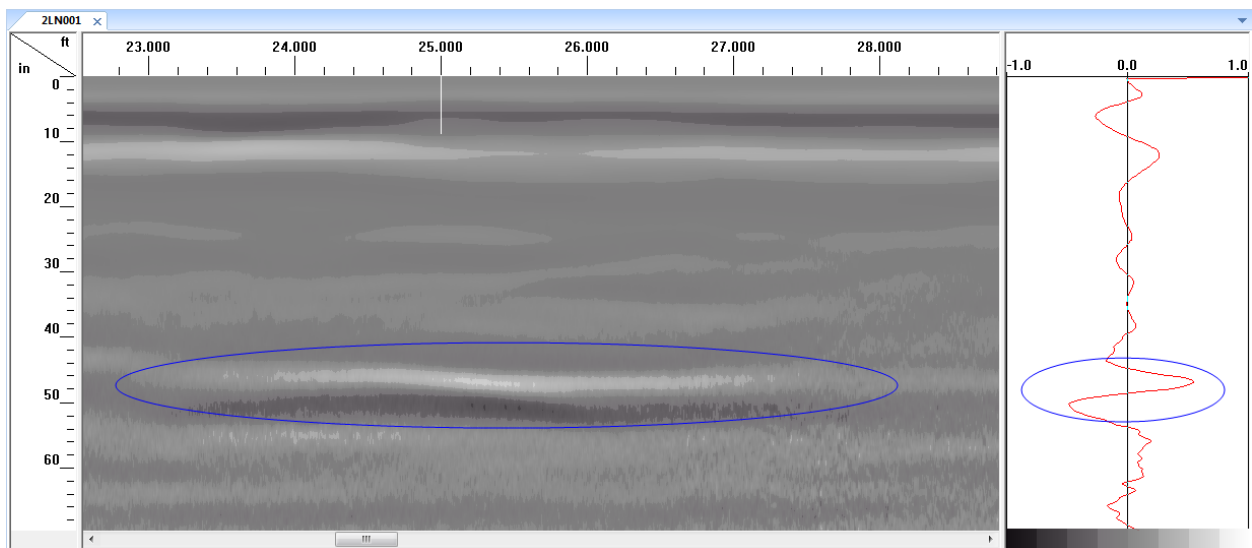


Figure 4-14: Longitudinal GPR scan (left) and A-Scan (right) over 12" CFRP Strip GFRP pipe

Figures 4-13 and 4-14 above show that the 12" diameter GFRP pipe with CFRP Ring or Strip show up prominently in the GPR scan.

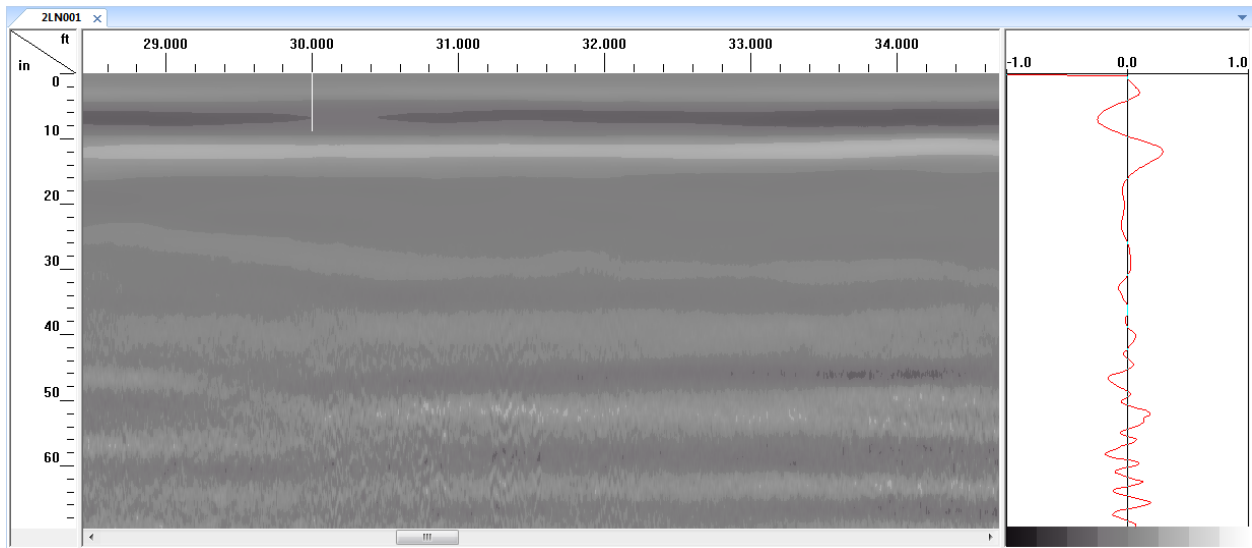


Figure 4-15: Longitudinal GPR scan (left) and A-Scan (right) over Unwrapped 12" PVC pipe

The Unwrapped 12" diameter PVC pipe buried at 3 ft. depth was not visible in raw image (Figure 4-15), but has a better visibility in processed image as shown earlier in Figure 4-9.

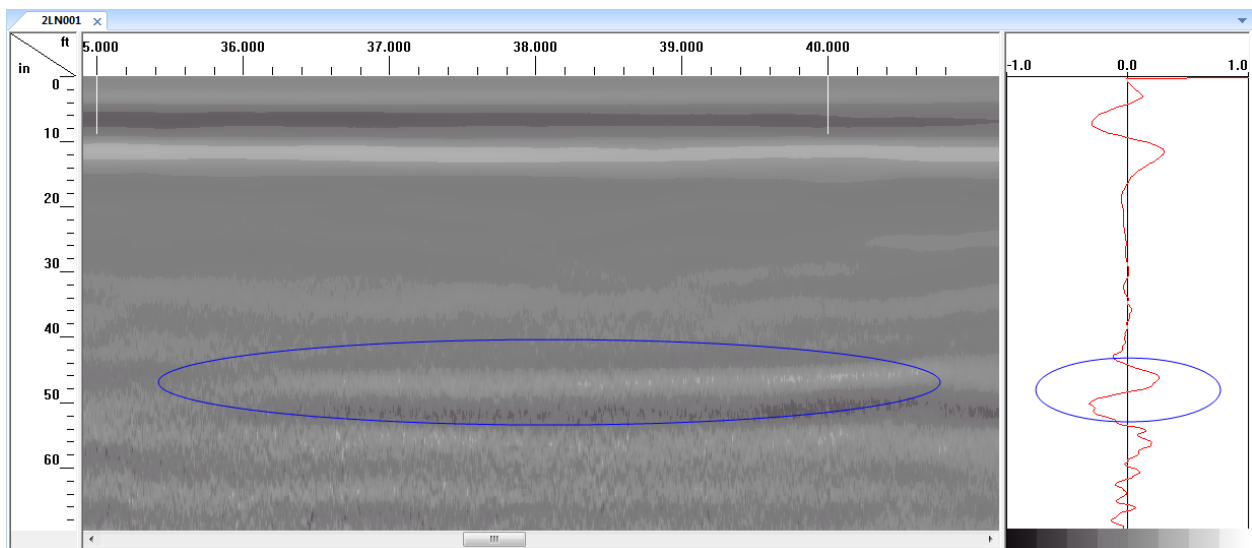


Figure 4-16: Longitudinal GPR scan (left) and A-Scan (right) over Al. Foil Ring 12" PVC pipe

The 12" diameter PVC pipe wrapped with Al. Foil Ring was only slightly visible in the raw image (Figure 4-16), but with a better visibility in processed image as shown earlier in Figure 4-9. The corresponding pipe with Al. Foil Strip (Figure 4-17) shows a more prominent GPR signal.

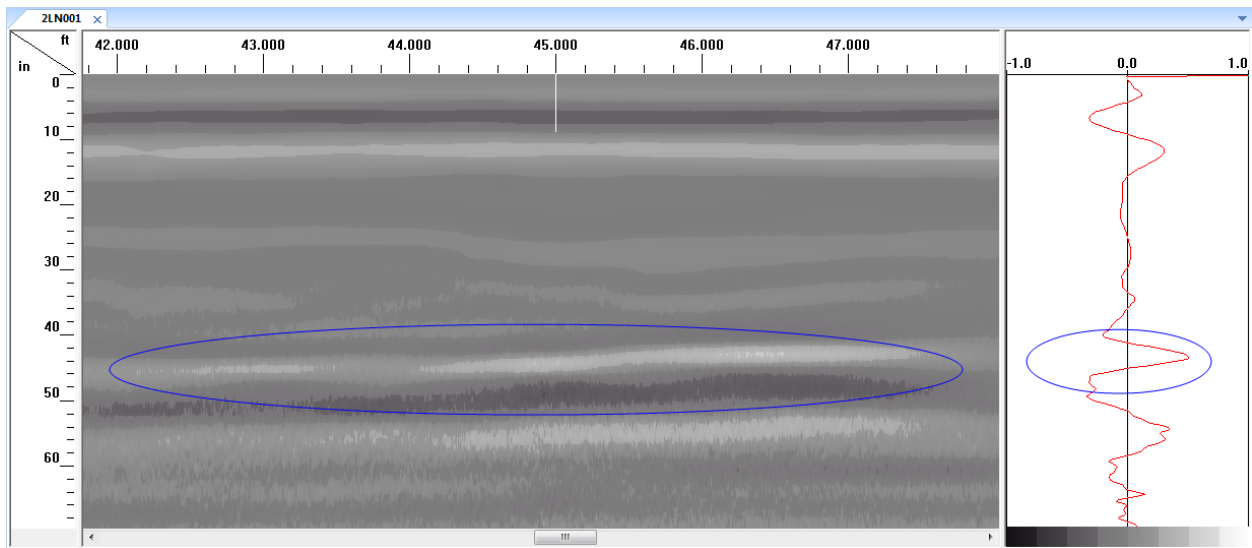


Figure 4-17: Longitudinal GPR scan (left) and A-Scan (right) over Al. Foil Strip 12" PVC pipe

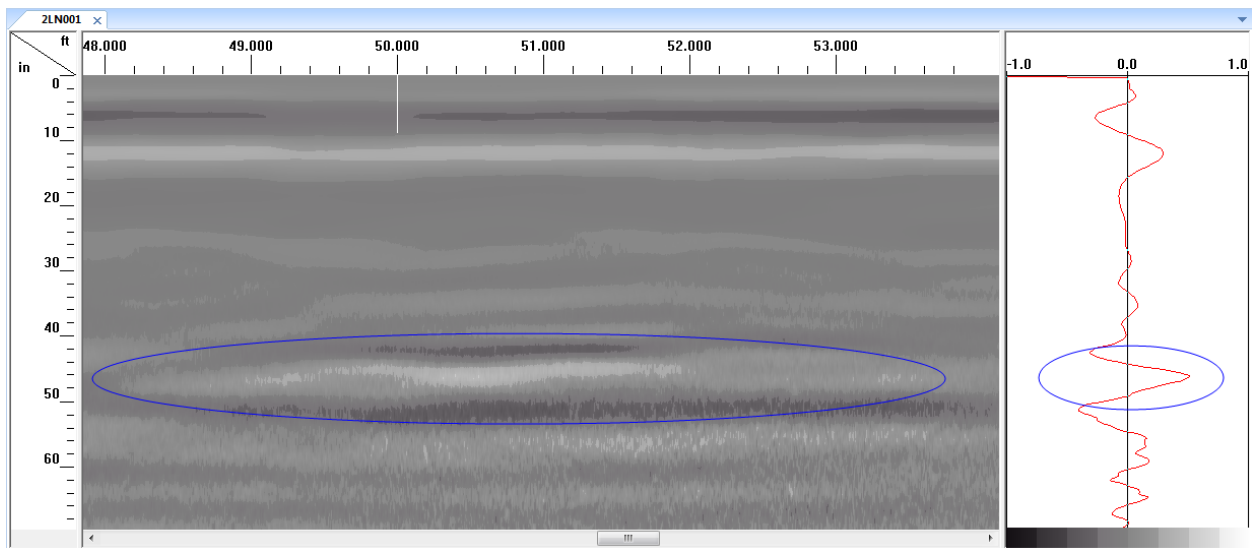


Figure 4-18: Longitudinal GPR scan (left) and A-Scan (right) over Unwrapped 6" PVC pipe

A comparison of GPR signals between the three cases of 6" diameter PVC pipes (unwrapped, and with aluminum foil ring or strip) shown in Figures 4-18, 4-19, and 4-20 indicates that the PVC pipe with the Aluminum Foil Strip on the top is the most prominently detectable configuration as indicated by the high strength of GPR signal in the A-scan in Figure 4-20.

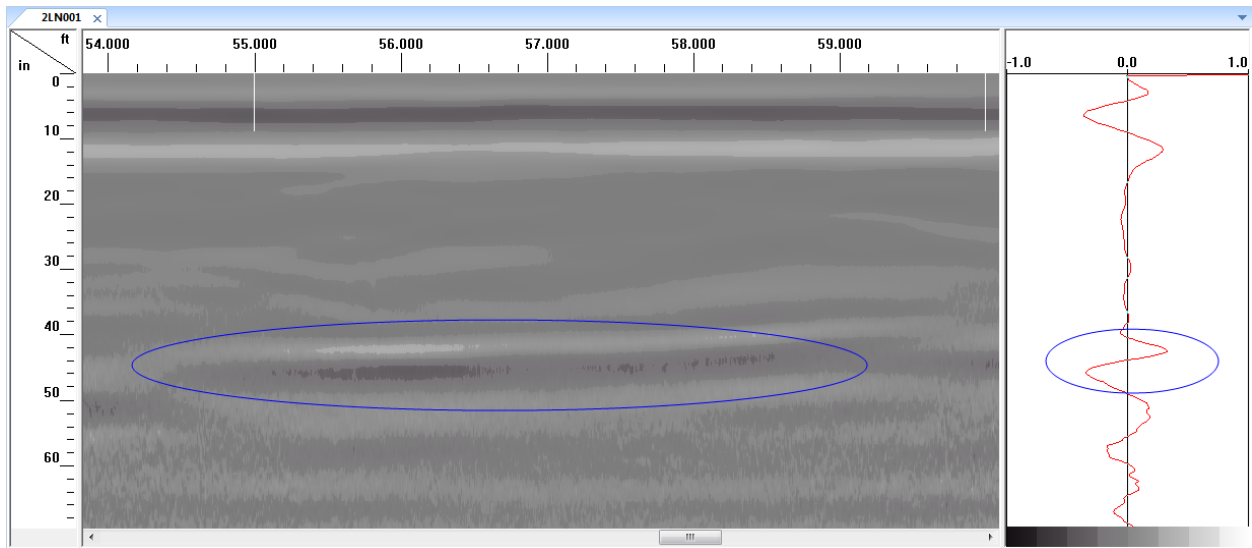


Figure 4-19: Longitudinal GPR scan (left) and A-Scan (right) over Al. Foil Ring 6" PVC pipe

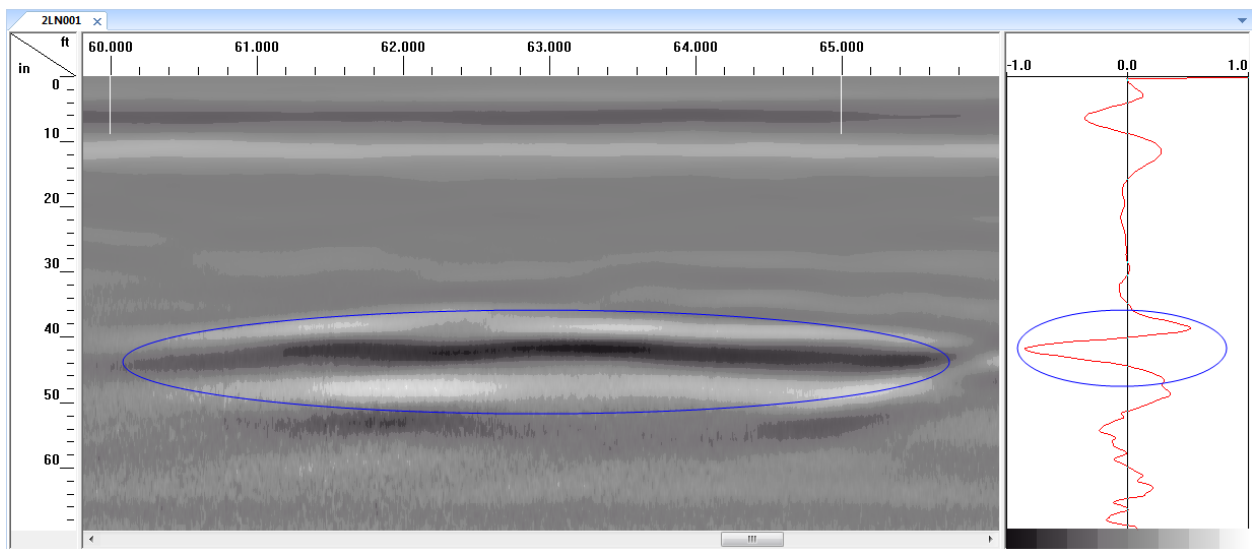


Figure 4-20: Longitudinal GPR scan (left) and A-Scan (right) over Al. Foil Strip 6" PVC pipe

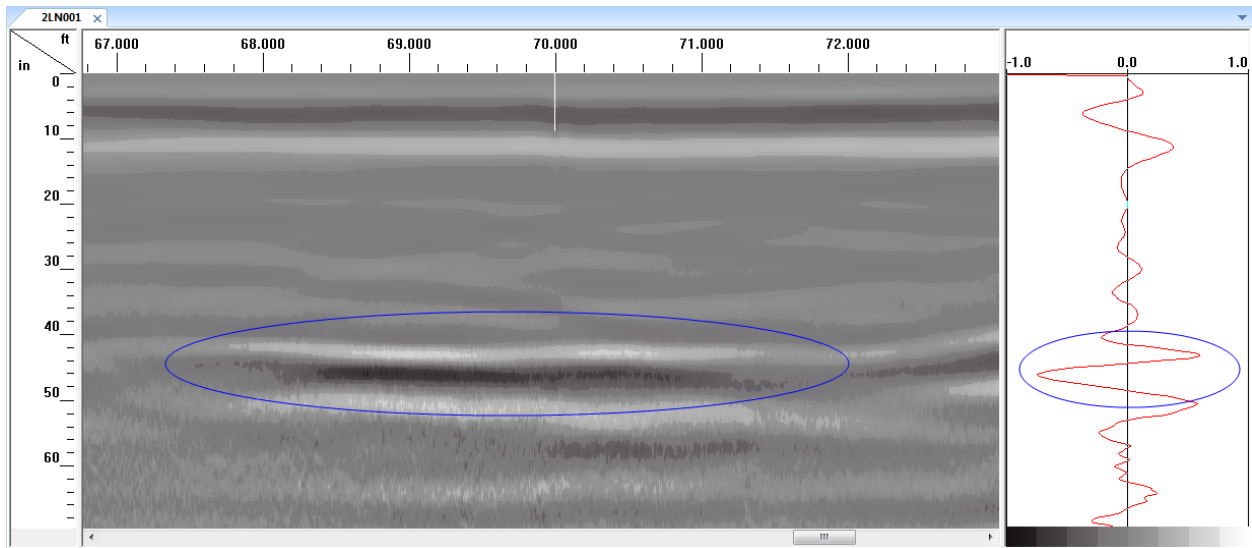


Figure 4-21: Longitudinal GPR scan (left) and A-Scan (right) over CFRP Ring 6" PVC pipe

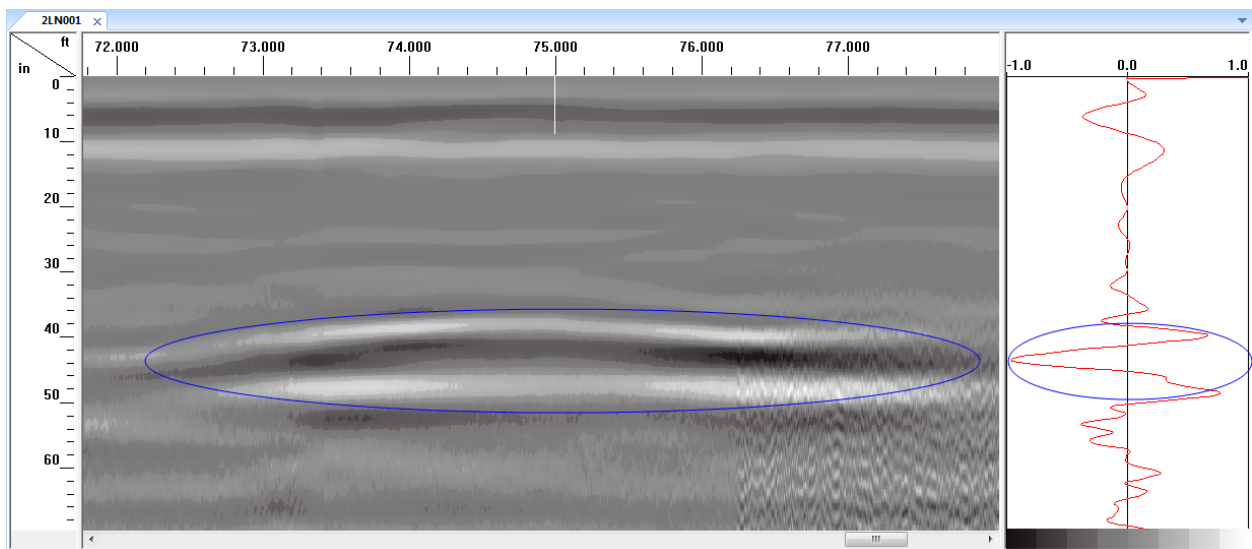


Figure 4-22: Longitudinal GPR scan (left) and A-Scan (right) over CFRP Strip 6" PVC pipe

Figures 4-21 and 4-22 show two cases of 6" diameter PVC pipes (wrapped with CFRP ring or strip). Both configurations are easily detectable but the one with CFRP strip (Figure 4-22) resulted in a higher strength of GPR signal.

4.4 Conclusions

From the GPR test data presented in this chapter, it can be concluded that, the use of CFRP and Aluminum foil overlays (in the form of rings and strips) improves the detectability of buried non-metallic pipe sections such as GFRP and PVC. The result in Datasets II and III demonstrate that, when the buried Unwrapped GFRP and PVC pipes are not detectable with GPR, addition of carbon fabric or aluminum foil overlays make them detectable. In cases where the buried Unwrapped GFRP and PVC pipes were detectable (albeit with faint and difficult to interpret signals), the addition of carbon or aluminum foil overlays significantly increases the strength of the GPR signal and makes it easier to identify the pipe sections.

The production of strong and easier to interpret GPR signals from buried non-metallic pipes with carbon fabric or aluminum foil overlays also implies that, the depth of pipe burial can be increased beyond the 4 ft. maximum depth used in this research and still adequate GPR signal strength could be obtained.

It is observed from this study that, carbon fabric overlays produce stronger signals compared to aluminum foil overlays. Additionally, it is observed that carbon fabric and aluminum foil “strips” generally produce better/stronger signals compared to carbon fabric and aluminum foil “rings” around non-metallic pipe sections.

5 IRT TEST SET UP AND RESULTS

5.1 Introduction

The feasibility of detecting subsurface pipelines (gathering lines) carrying hot liquid using Infrared Thermography (IRT) was explored in this research. Since petroleum products are hot in the initial part of the pipeline (within about 5 miles from the source of production wells), the IRT technique offers some promise for detecting such pipeline sections.

5.2 IRT Camera and Thermocouples

FLIR InfraCAM SD thermal imager (Figure 5-1 (a)) was used for the IRT testing. This is a portable handheld infrared camera with a spectral range of 7.5 to 13 μ m, a 0.12°C thermal sensitivity at 25°C, and \pm 2°C accuracy.



(a) FLIR InfraCAM SD camera

(b) Digi-Sense type-T thermocouple

Figure 5-1: FLIR InfraCAM SD camera and type-T thermocouple

The Digi-Sense type-T thermocouple probe (WD-08519-54, shown in Figure 5-1(b)) was used for contact temperature measurements. A 1"x2" high temperature self-adhesive tape was used to attach the thermocouple to the pipe surface during testing. The thermocouple has a temperature range of -200°C to 260°C and a \pm 1.0°C accuracy for readings above 0°C.

5.3 Experimental Set-Up for IRT Testing

An insulated wooden box with an internal dimension of 24"x24"x22" (after insulation) was built for the IRT testing of buried CFRP pipe carrying hot liquid. The insulation in the box (with R-Value of 10) will ensure that heat detection (if any) will only be as a result of heat propagation from the hot pipe to the soil surface. Also, the insulation ensures no heat leakage out of the box, which will help in heat transfer computations to extrapolate the surface temperature for different soil depths. Figures 5-2 and 5-3 show the wooden box and capped 3" diameter CFRP pipe respectively. The CFRP pipe, fitted with aluminum caps was buried in the insulated box with hot water circulated through the pipe

The pipe was buried in the box filled with a mixture of gravel, sand, and top soil in the ratio of 1:1:2, and having a moisture content of 14%. 3" of the soil mixture was placed at the bottom of the insulated box before the pipe was inserted. Soil cover above the pipe was 14", and 2" space was left at the top of the box as shown in Figure 5-4. The box was left open at the top (no top cover) during the experiments to simulate field conditions where the soil surface is exposed.

Five thermocouples were installed on the surface of the CFRP pipe before burying (3 thermocouples at the top and 2 at the bottom surface of the pipe). Another thermocouple was placed at the surface of soil in the box to measure soil surface temperature. Hot water (at a temperature of 95°C) was circulated through the buried pipe, while the temperature changes at the surface of the buried pipe and the soil surface were recorded over a period of 10 days. Soil surface temperature was also recorded using infrared thermography (IRT) throughout the testing period. It should be noted that, water circulation was started with the water initially at room temperature (21.6°C), and it took 3 hours for the water temperature to rise to the 95°C level. Also, the hot water did not fully fill the pipe to the top, hence top portion of the pipe was colder than the bottom portion by about 4.5°C because of the trapped air pocket at the top. The IRT test setup is shown in Figures 5-4.



(a)



(b)

Figure 5-2: Insulated wooden box used for IRT testing



Figure 5-3: Capped CFRP pipe used for IRT testing

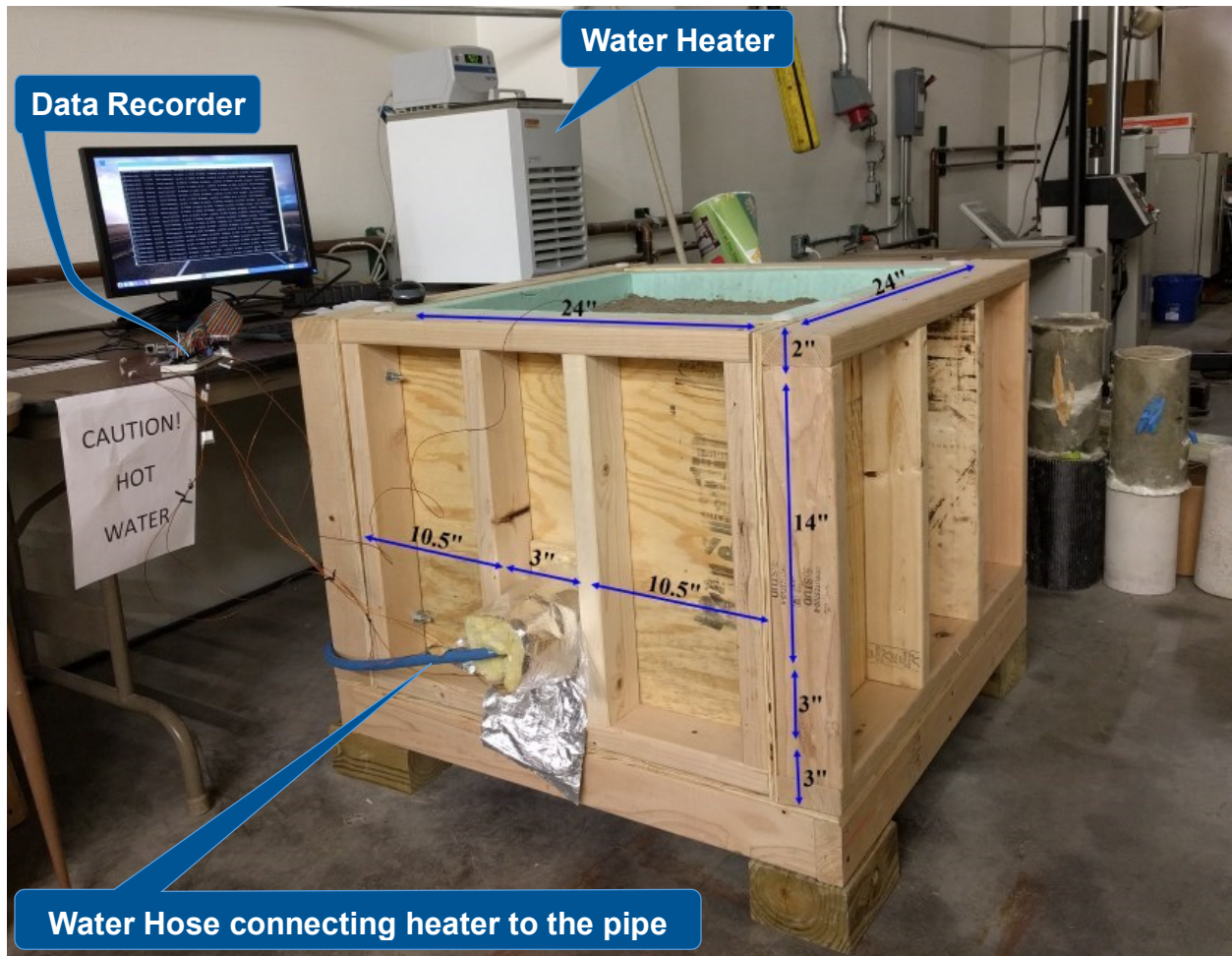


Figure 5-4: IRT test set-up

5.4 IRT Test Results

As stated previously, the IRT test was carried out over a period of 10 days where hot water at a temperature of 95°C was circulated through the buried 3" CFRP pipe. The temperature at the pipe and soil surfaces, and room/ambient temperatures were recorded over the testing period. Temperature at the soil surface had a sharper increase during the first 48 hours of testing, followed by a gradual increase up to the sixth day of testing. There was not much temperature increase between the sixth and tenth days of testing. Figure 5-5 shows some of the IRT data at various stages of testing. Figures 5-6 and 5-7 show plots of temperature changes during the test period. The results (IRT curve in Figure 5-6) show approximately 14°C increase in surface temperature of the soil for this pipe carrying hot liquid, thus making it possible to detect such buried pipes using infrared thermography measurements at the soil surface. Infrared thermography readings at the soil surface were found to be about $2\text{--}3^{\circ}\text{C}$ higher than the thermocouple readings at the same location. This can

be explained by the $\pm 1.0^{\circ}\text{C}$ accuracy of the thermocouples which is less accurate than the $\pm 0.12^{\circ}\text{C}$ accuracy offered by the infrared camera measurements.

The following nomenclature are adopted to explain the IRT data in Figures 5-6 through 5-8:

- IRT** – Infrared thermography image/data/temperature reading
- TSC** – Thermocouple reading taken at the center of the soil surface
- Amb** – Ambient/room temperature
- TSC-Amb** – Difference between TSC and Amb
- IRT-Amb** – Difference between IRT and Amb

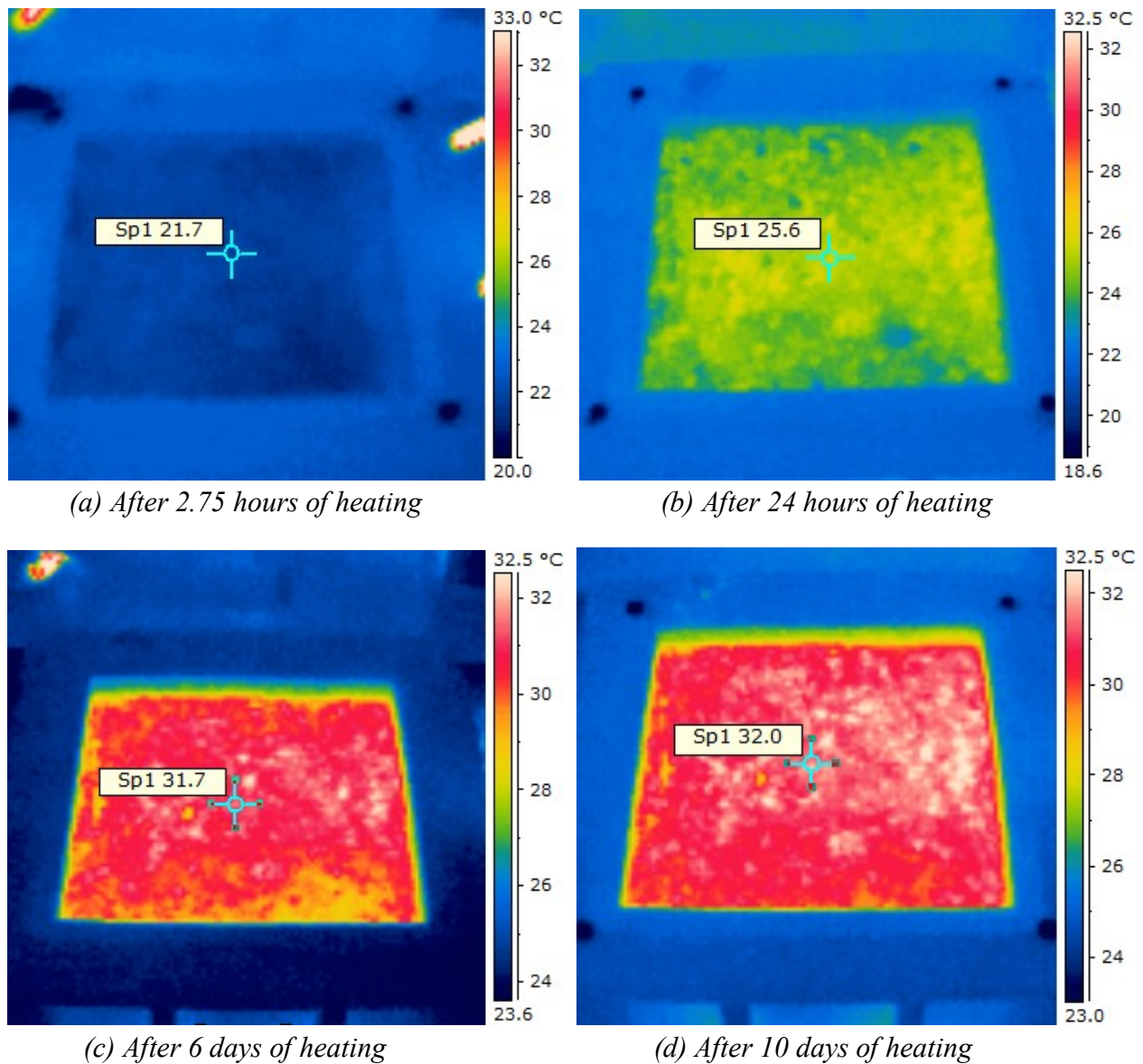


Figure 5-5: Infrared thermography data at the soil surface at various stages of testing

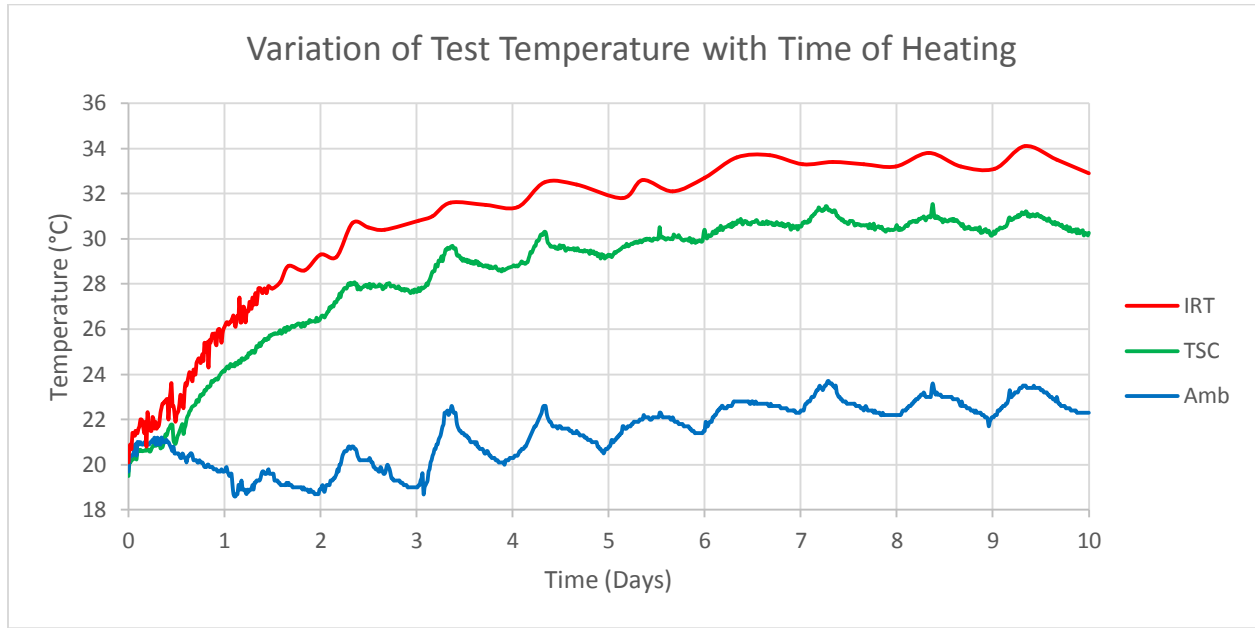


Figure 5-6: Variation of soil surface (TSC, IRT) and room (Amb) temperatures with time

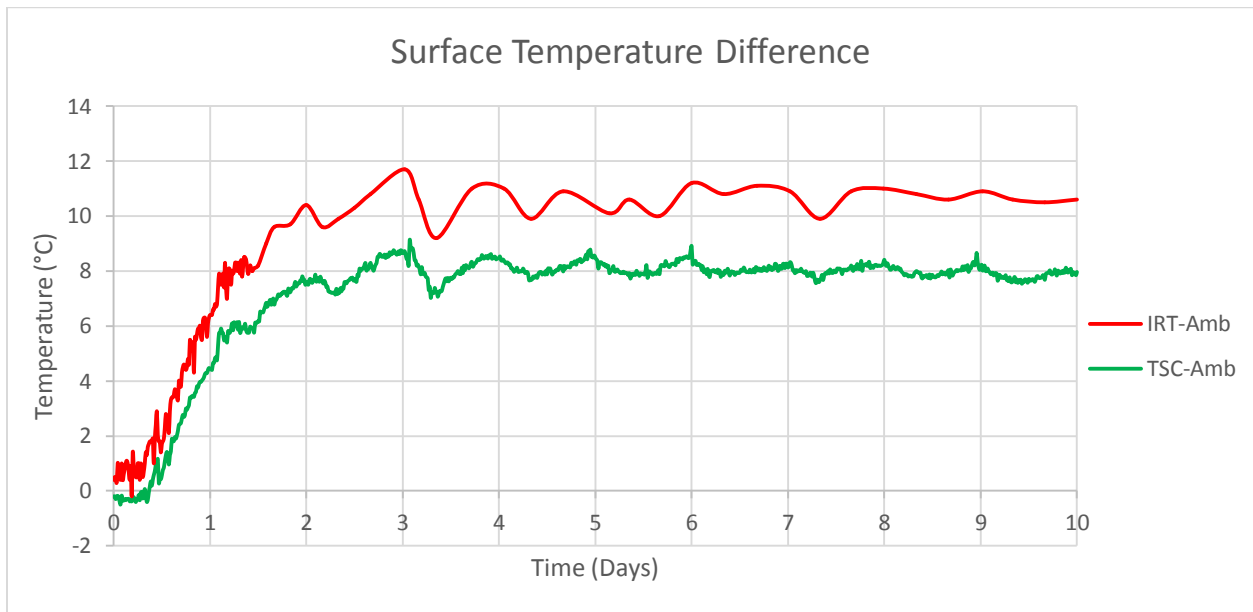


Figure 5-7: Soil surface temperature difference with time

The results show that, the 3" diameter CFRP pipe buried with 14" of soil cover and carrying 95°C of liquid can be detected at the ground surface using infrared thermography. The results were extrapolated using a one-dimensional heat transfer (conduction) formulation to estimate the depth

at which the pipe will no longer be detectable using IRT. The heat transfer equation for one-dimensional heat conduction is given by Equation 5-1.

$$q_{net} = \frac{k}{d}(T_h - T_c) \quad (5-1)$$

where,

q_{net} = net heat flow through a unit area of a material per unit time (W/m²)

k = thermal conductivity of the medium (W/m/°C)

T_h = temperature of the hotter side (°C)

T_c = temperature of the colder side (°C)

d = thickness/depth of the medium (m)

The ratio q_{net}/k was assumed to be constant for the soil mixture during the computation. The experimental data at day 6 was used as a baseline for this computation because the system had reached a steady state by that time as illustrated by the almost constant temperature difference in Figure 5-7. All temperatures in this computation are from thermocouples readings:

q_{net}/k = assumed constant (and computed by using the following data)

T_h = Temperature at the surface of the buried pipe at day 6, measured to be 85.47°C

T_c = Temperature at the surface of the soil at day 6, measured to be 30.40°C

d = depth of soil cover over the pipe, 14"

Soil surface temperature difference (difference between soil surface temperature and room temperature or TSC-Amb) for different depths of soil cover were computed and the result is plotted (Figure 5-8). Figure 5-8 also shows the projected temperature difference using IRT (IRT-Amb), which is higher than TSC-Amb by 2.5°C at each data point. The plot in Figure 5-8 shows that, the same 3" CFRP pipe buried in the same soil medium and carrying a liquid at 95°C will be detectable using IRT, up to a depth of about 16.5"; with a temperature increase of about 1.6°C.

5.5 Conclusions

The IRT test conducted in this research demonstrate that, buried pipe transporting hot liquid such as petroleum products from production wells or refinery plants have the potential of being

detectable using IRT. The results show that, IRT can be used to detect the 3" CFRP pipe up to a depth of 16.5" in the test medium when 95°C water is pumped through the pipe.

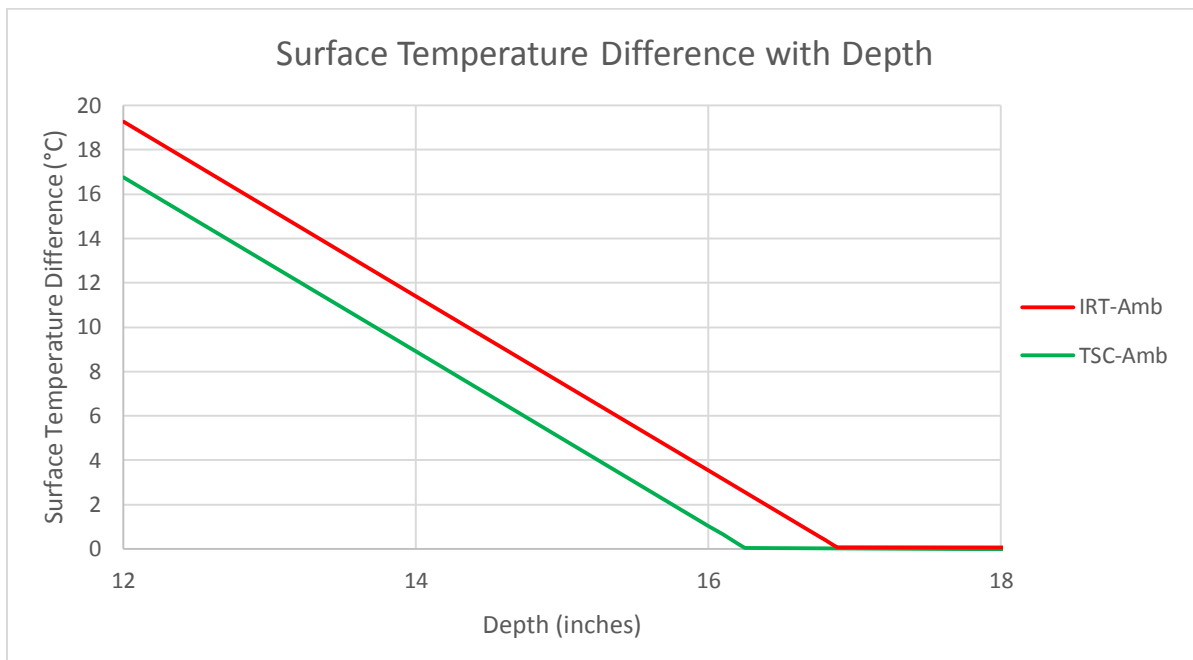


Figure 5-8: Difference between soil surface temperature and room temperature with depth

Tests and computations in this chapter assumed a one-dimensional heat conduction equation to arrive at the depth of possible pipe detection. Heat transfer in the field environment will not be one-dimensional, but rather three-dimensional. Also, bigger diameter pipes (much bigger than 3") are used in the field to transport petroleum products at temperatures less than or equal to 200°F (93°C). This temperature is about equal to what was used in the laboratory test (water temperature was 95°C, but trapped air pocket above the water in the pipe reduced the pipe surface temperature at the top of the pipe by 4.5°C compared to the pipe surface temperature at the bottom of the pipe). The three-dimensional heat transfer in the field environment will reduce the depth of pipe detection to an extent, but the use of bigger diameter pipes is expected to have a bigger effect in increasing the depth of possible detection using IRT.

Thus, IRT has the potential of being used in detecting pipelines transporting hot liquids, but the maximum depth at which the pipe can be detected will depend on the diameter of the pipe and the temperature of liquid being transported.

6 GAS LEAK TESTING

6.1 Introduction

Utility production, transportation, and distribution drives the economy like few other forces. In the United States alone, there are over 3 million miles of oil, gas, and other utility pipelines buried underground. When these pipelines are buried, it is essential that an accurate mapping of their location be made to prevent damage to the lines, as well as to avoid accidentally rupturing the lines which could result in an emergency situation. Within the United States, many of these pipelines are falling into disrepair due to old age, and it has become necessary to revamp this infrastructure system (Groeger 2012).

A major facet of this revamp is the modernization of the materials with which the pipelines are constructed. These modern materials are not made of metal, and, as a result, are difficult to detect underground and accurately map by traditional means. The focus of this chapter is to investigate the mapping of the new piping materials in buried condition by detecting the small amounts of gas leakage from these pipes. This work involves the development of methods for the detection of underground leaks. These new methods and techniques will be used to detect the pipes themselves and also guarantee the structural integrity of the piping system.

6.2 Test Set-Up

Initially it was decided to simulate a leaking buried pipe by constructing a wooden box into which a pipe of up to six inches in diameter could be inserted. The box was then filled with crushed stone and dirt to bury the pipe. The pipe had a tiny hole drilled in its wall to simulate a gas leak underground. The first wooden box which was constructed for gas leak detection was filled with highly saturated clay that was not porous once it dried, preventing the gas from flowing through the clay and out of the top of the box. But rather than dig all the non-porous soil out of the old box, it was decided to build a new wooden box for conducting additional experiments. This new box, shown in Figures 6-1 (a), 6-1 (b), and 6-1 (c), was constructed with several improvements over the previous box. All of the seams were sealed with a silicone caulking, the inside of the box was lined with a three millimeter plastic lining and the soil being placed in the box was hand-mixed with sand, gravel, and top soil at a ratio of 1:1:2 respectively. A new eight-inch diameter aluminum pipe

was placed near the bottom of the box to allow for easy insertion and removal of test pipes, and reducing “Fernco” fittings are being used to create a better seal between the aluminum pipe and the test pipe. Overall, the new box will provide a better representation of gas flow through a porous medium, and therefore be a better mimic of an underground pipe leak. The box is currently half full with the hand mixed soil, and tests are being run to ensure that carbon dioxide, the gas used for the leak detection, is leaking through PVC test pipe and the soil, and being detected by the mass spectrometer (see description below) attached to the top of the box.

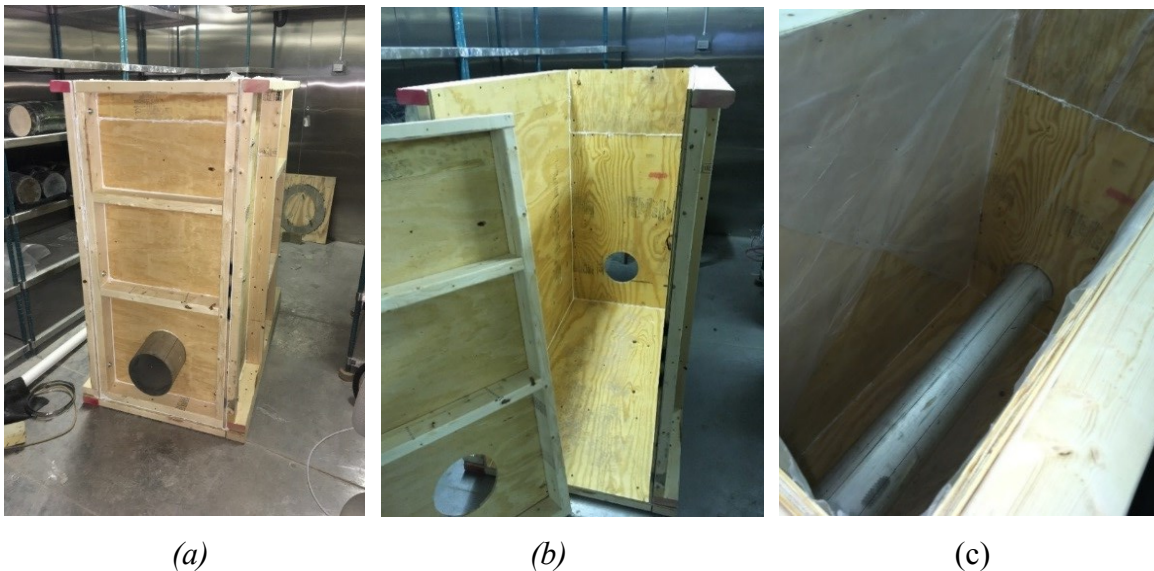


Figure 6-1: (a) New wooden box, showing caulked seams, (b) Interior of assembled box, and (c) Exterior of assembled box

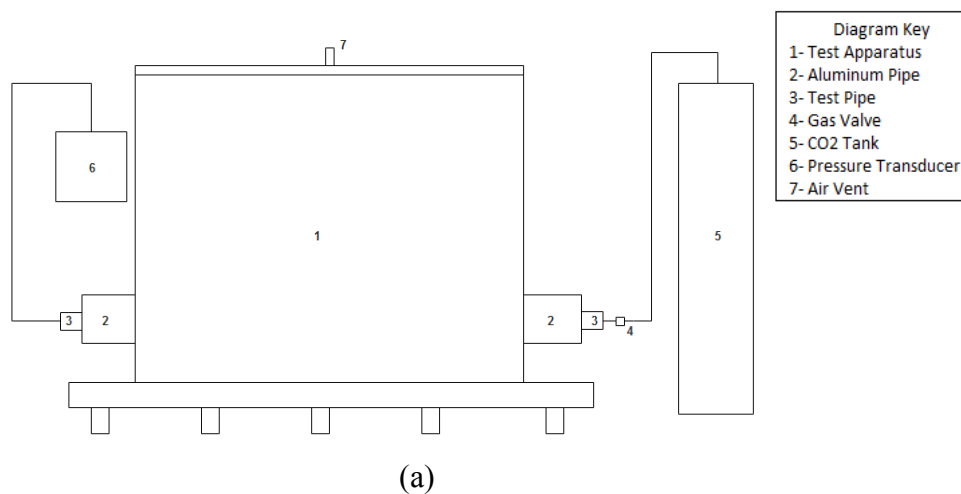
Before any experimental trials could be conducted, a model pipe was selected. The chosen piping material for this model was a standard 2" PVC pipe roughly 56" long to allow for overhang outside of the aluminum pipe. This overhang was necessary to allow for the Fernco seal to be placed around outside of the PVC pipe that could also fit around the edge of the aluminum pipe as well. The rubber seals were secured around the outside of both the 8" and 2" pipes with standard hose clamps. To accurately measure the pressure inside the test pipe, an Omega PX409-100GUSBH pressure transducer was connected to one end of the PVC pipe. The transducer is capable of measuring pressures up to 100 psig and is accurate to $\pm 0.08\%$, which is extremely accurate. A cylinder of carbon dioxide (CO_2) was connected to the other end of the pipe. Carbon dioxide was selected since it is non-toxic and readily available. A valve was placed in-line with the inlet from the CO_2 tank that would allow the system to be filled with CO_2 and then closed off, or isolated,

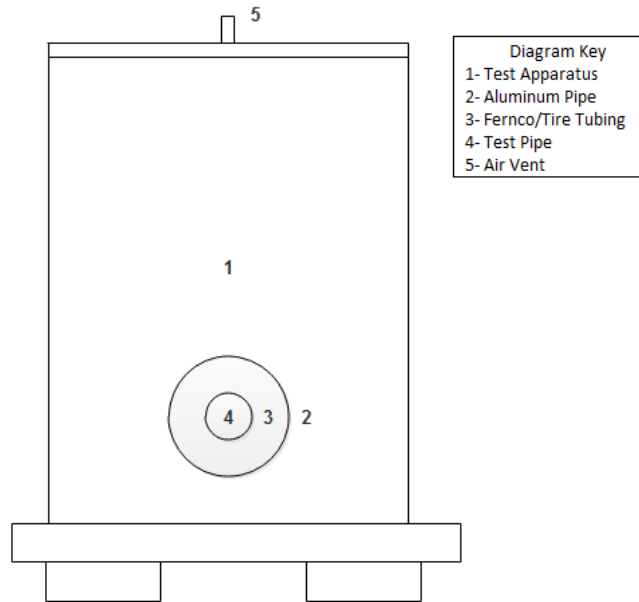
from the CO₂ tank. A pressure regulator was installed on the CO₂ cylinder to allow the pressure inside the test pipe to be controlled precisely. Figure 6-2 shows the CO₂ tank, not pictured is the gas valve pictured in Figure 6-3, but it is a simple quarter inch ball valve.



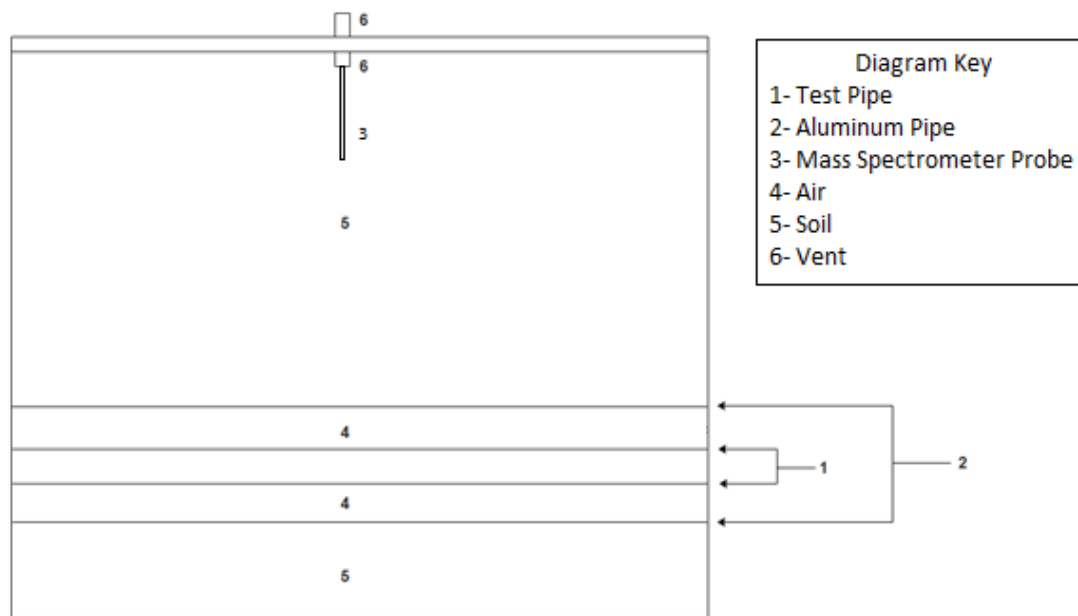
Figure 6-2: *CO₂ Cylinder and Pressure Regulator*

A hole with a diameter of 0.0135 inch (No. 80 drill bit) was drilled into the mid-point of the length of PVC pipe to allow for the simulation of a gas leak in the system. Figures 6-3 (a), (b), and (c) display more detailed schematics of the testing apparatus.





(b)



(c)

Figure 6-3: (a) Testing apparatus schematic diagram side view, (b) Testing apparatus schematic diagram end view, and (c) Testing apparatus schematic, interior view

To detect and measure the quantity of the CO₂ leaking from inside of the PVC pipe, additional gas-sensing equipment was needed. The chosen experimental apparatus was an on-line mass spectrometer. The mass spectrometer used for this analysis was the *LM99 Cirrus*, manufactured by MKS Instruments. The mass spectrometer can detect low quantities of CO₂ (down to parts per million) in the air, and was used to measure the concentration of CO₂ inside of the housing apparatus once the CO₂ from the tank was released into the apparatus and the leak simulation tests began. Figure 6-4 shows the mass spectrometer as well as the computer necessary to operate it.

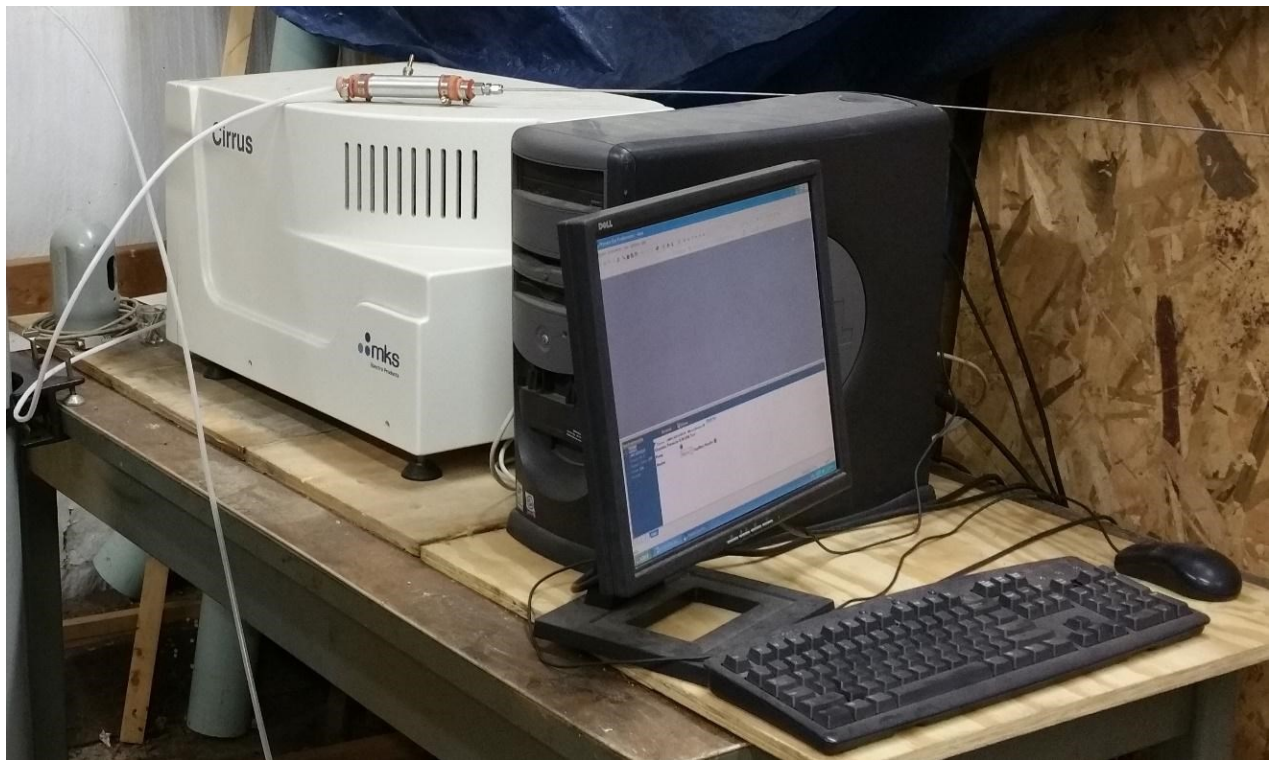


Figure 6-4: Mass spectrometer and associated experimental equipment.

6.3 Test Results

Tests have been performed to obtain data on detecting the leak in the pipe installed in the box filled with porous soil. To do this, the pressure gauge was set at a steady flow rate and left to run so that the concentration of CO₂ increased drastically inside the test box. This increase is shown Figure 6-5. As can be seen, the mass spectrometer did indeed detect the leak of carbon dioxide when its probe was placed directly near the top level of the soil. A plot of the detector counts (in arbitrary units) vs. time is shown in Figure 6-5.

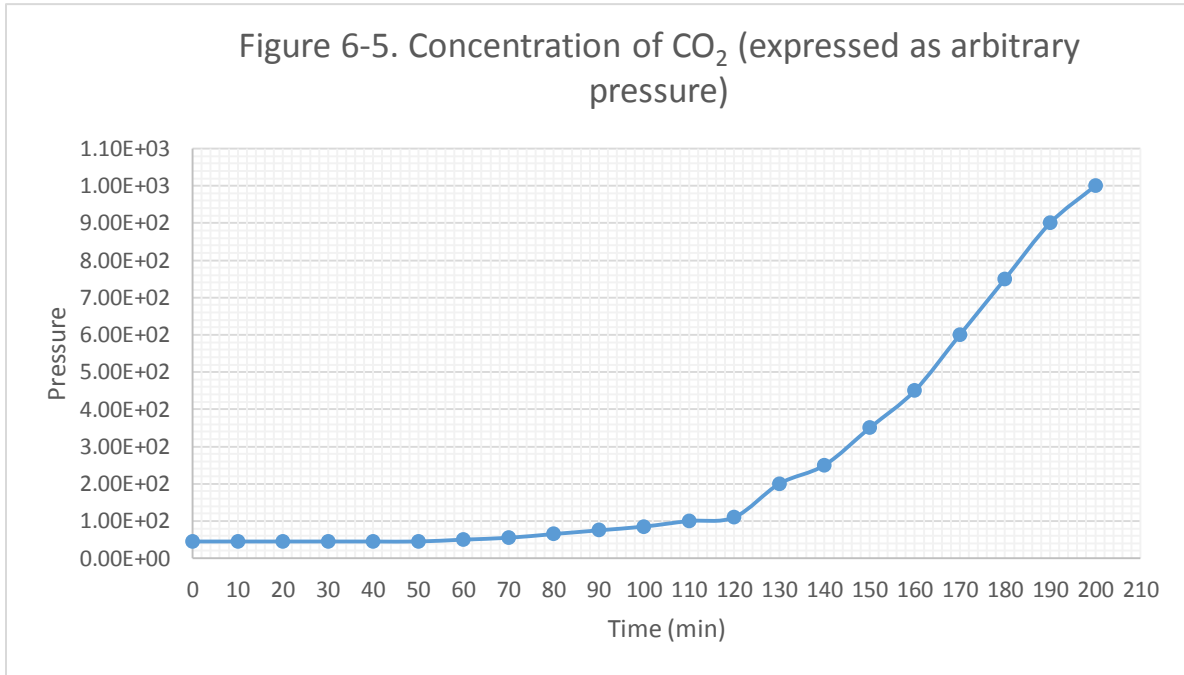


Figure 6-5: Concentration of CO₂ as a function of time for a leak in the test pipe (expressed as arbitrary pressure)

Trials have also been run to ensure that the leak rate out of the hole drilled in the test pipe coincides with the theoretical calculated leak rate. Since the mass flow rate out of the PVC pipe is choked, the equation used to model the flow rate through the leak hole in the PVC pipe is:

$$\dot{m} = C_0 A P(t) \sqrt{\frac{\gamma g_c M}{R T_0} \left(\frac{2}{\gamma + 1} \right)^{\frac{\gamma + 1}{\gamma - 1}}} \quad (6-1)$$

where:

\dot{m} = Mass Flow Rate

C_0 = Discharge Coefficient

A = Area of Leak Hole

$P(t)$ = Pressure in the Pipe in psia with respect to time

γ = Heat Capacity Ratio of the Gas

g_c = Mass/Force Conversion Factor

M = Molecular Weight of the gas

R = Universal Gas Law Constant

T_0 = Absolute Temperature of Gas

Equation 6-1 was then simplified to:

$$\dot{m}(t) = KP(t) \quad (6-2)$$

Where K is a collection of constants:

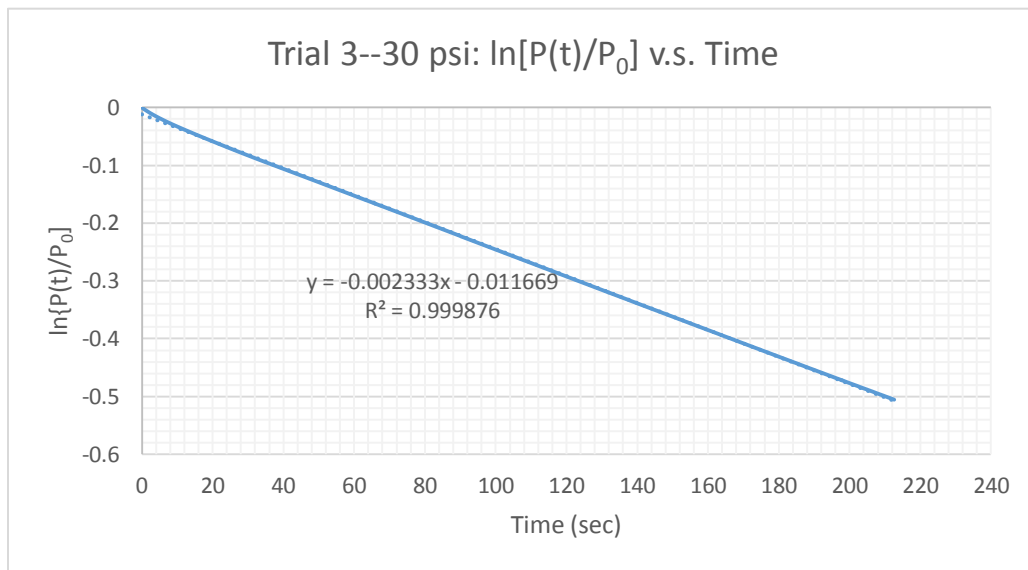
$$K = C_0 A \sqrt{\frac{\gamma g_c M}{RT_0} \left(\frac{2}{\gamma+1} \right)^{\frac{\gamma+1}{\gamma-1}}} \quad (6-3)$$

It was possible to do this simplification because all the parameters in Equation 6-1 are constants except for the upstream pressure in the pipe and the mass flow rate. This creates a direct and simple relationship between the mass flow rate and starting pressure induced in the pipe. Also, since the pressure inside the pipe can vary with time, the equation captures the linear relationship between the transient mass flow rate and the pressure provided that the flow stays in the choked regime. The collection of constants, K , was calculated to be $2.647 \times 10^{-6} \frac{lb \cdot m}{sec \cdot psia} \cdot P$. Further since the mass flow of a gas can be related to the gas pressure, it is possible to integrate Equation 6-2 and derive an expression for the pressure as a function of time as the gas leaks from the pipe. The resulting expression for the internal pressure vs. time is shown in Equation 6-4.

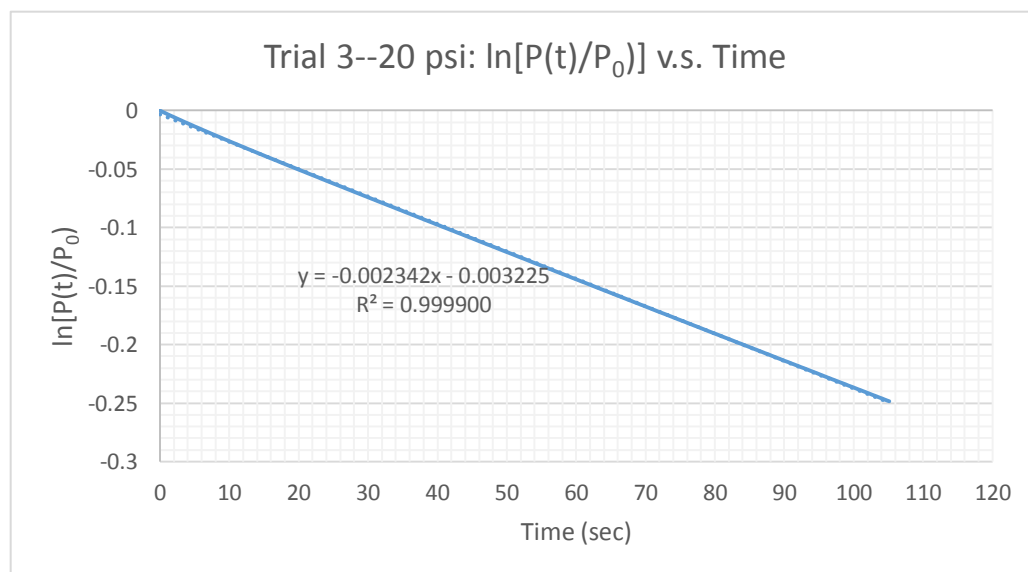
$$\ln \left(\frac{P(t)}{P_0} \right) = -kt \quad (6-4)$$

The simplest way to validate the theoretical assumption of choked flow was to plot the natural log of the transient pressure divided by the initial pressure versus time and plot a line of best fit. The slope of the best fit line is directly to the variable, k , from Equation 6-4. Using the “ k ” value

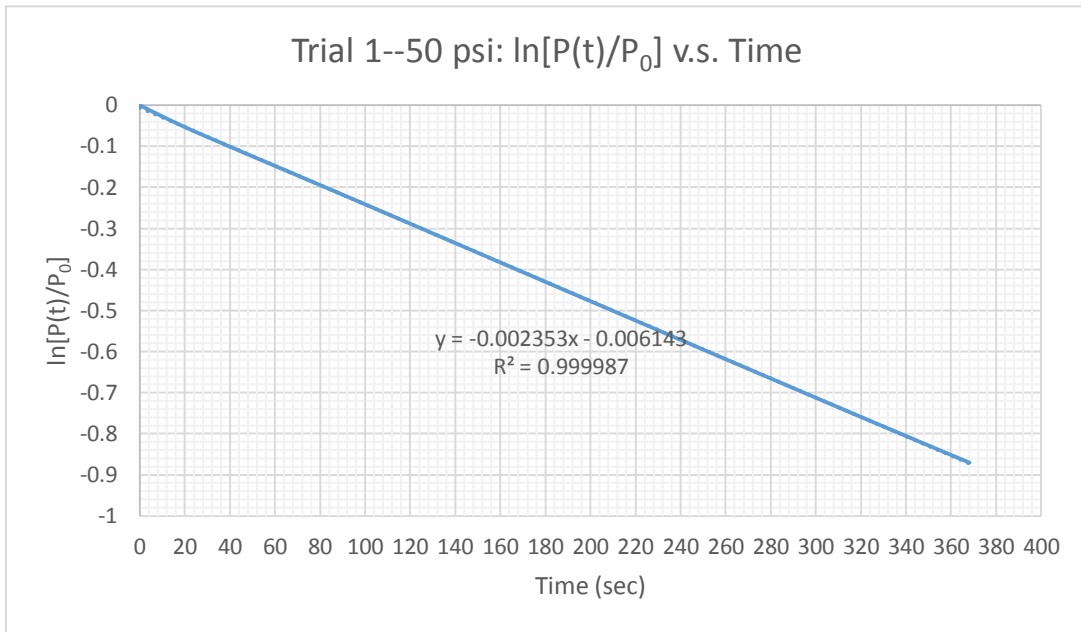
determined from the plots mentioned above, it is possible to back calculate the “K” value from Equation 6-2. Since all the values from the aforementioned plots were within five percent of the k value of $2.34 \times 10^{-3} \text{ sec}^{-1}$, this validates this part of the experiment and will allow for this part of the project to move forward. Some of the experimental results are shown in the following Figure 6-6 (a), (b), (c), and (d).



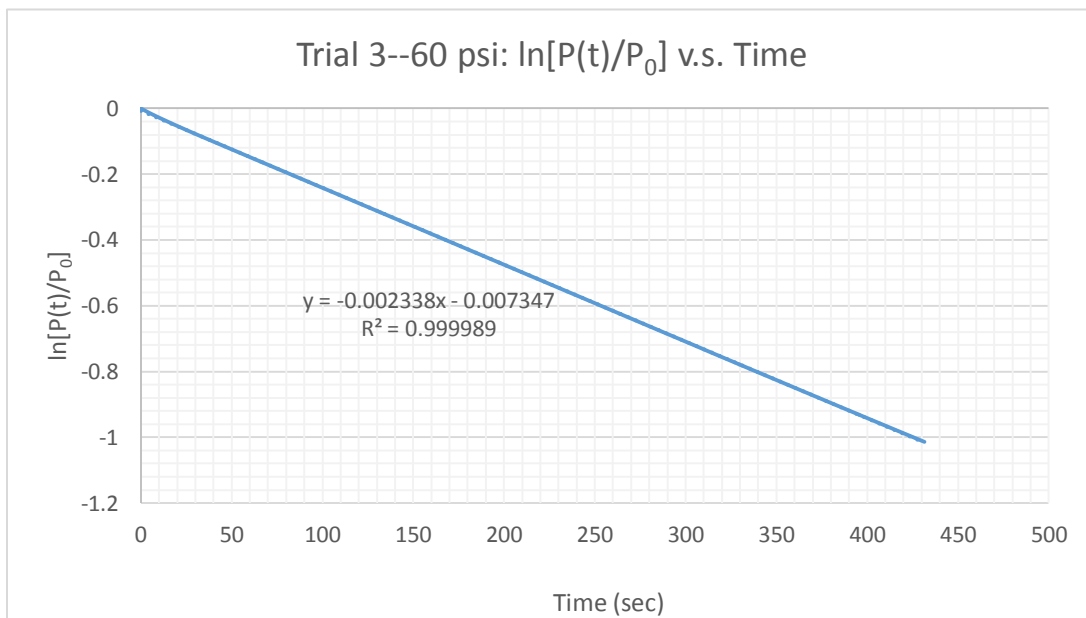
(a)



(b)



(c)



(d)

Figure 6-6; (a), (b), (c), (d): All represent the titles given to each with the starting pressure for the shown trial listed after the trial number. The slope of the best fit lines represents the experimental “k” values mentioned in the text above.

6.4 Conclusions

After analyzing the data and creating the above plots, it was determined that our “K” value was more than acceptable when compared to the theoretical “K” value. The experimental value is determined by the absolute value of the slope of the best fit line in the plots above and others like them. All the experimental “K” values from all the trials were within five percent of the theoretical value. This will become beneficial when a model for the gas flow through the soil is developed. It can also be used to estimate the size of a leak in a test section of composite pipe.

Conclusions that can be drawn from this research are that the mass flow rate out of the test pipe is in good agreement with the choked flow model and its assumptions. This will help create the one-dimensional diffusion model that will help determine the relationship between the diffusion of gas through the soil and the various levels of soil depth and compaction. A one-dimensional transient diffusion model can be used to fit the experimental data. This part of the research can also allow the back calculation of the size of the leak in the pipe if needed. The other conclusion that can be made is that we have a viable method for detecting a leak with the mass spectrometer as can be seen from Figure 6-5 with the increase in gas concentration inside the soil box.

7 BROADER IMPACTS

This project has helped to develop non-metallic Fiber Reinforced Polymer (FRP) composite pipes as possible replacement for steel pipes. The non-metallic FRP pipes are light-weight, possess high strength, and do not corrode in the buried environment. Strategies to detect such pipes using ground sensory technologies have also been successfully demonstrated.

The project work involved one Ph.D. student and several M.S. students who are now familiar with buried pipes, safe digging procedures, advanced composite technologies, etc. The Ph.D. student along with two M.S. students were lead participants in development and testing of composite pipes, buried pipe detection using Ground Penetrating Radar and Infrared Thermography, and Gas Leak Detection using an advanced Mass Spectrometer. These three lead graduate students (research assistants) were assisted by several other M.S. level graduate students in the testing process, thus familiarizing them with the pipeline industry and related issues. At least two of the three lead graduate students will graduate within the next 12 months.

One Ph.D. and one M.S. student attended the research forum held in Cleveland, OH during November 16-17, 2016. The Ph.D. student presented a poster showcasing his research work. Both students interacted with several industry participants and learnt the issues and challenges facing the pipeline industry. The Ph.D. student also attended the PIANC-SMART Rivers Conference held in Pittsburgh, PA during September 18-21, 2017 and presented a poster entitled, “Detection of Buried FRP Composite Pipes Using NDT Techniques.”

Preliminary results based on this project work revealed that buried FRP pipes can be detected using Ground Penetrating Radar up to 4’ below ground. Additionally, spectral analyses revealed small leaks of gas after capturing and analyzing air samples around a pipe. The internal pressure testing showed that current designs of FRP composite pipes are providing burst pressures up to 2300 psi and additional work is being carried out to improve burst pressures up to 10,000 psi.

In addition to making significant strides in advancing the technology related to manufacturing high pressure FRP pipes and their detection using ground sensory technologies, this USDOT-PHMSA funded research project has been immensely useful in training a number of graduate students, make them appreciate the requirements of the pipeline industry, raise awareness in the area of pipeline safety, and help them prepare for future work in pipeline related areas.

8 CONCLUSIONS

Advanced non-metallic composite pipe materials such as Glass Fiber Reinforced Polymer (GFRP) have desirable engineering and mechanical properties that can help address some of the challenges encountered in the pipeline transportation industry. However, limitations such as difficulty in locating buried GFRP pipe, and the need for design to withstand high burst pressures, are preventing the adoption of such materials in the pipeline industry. This project has investigated alternative strategies for creating easily locatable non-metallic pipe material.

Through internal pressure testing it is concluded that current designs of FRP composite pipes are providing burst pressures up to 2300 psi and additional work is being carried out (as a part of another USDOT-PHMSA funded project) to improve burst pressures up to 10,000 psi. Furthermore, additional work is being carried out on joint design and testing to increase the joint burst pressures up to 20,000 psi, since joints must be twice as strong as the pipes. Burst pressures in these ranges would allow composite pipelines to operate at pressures near 2000 psi, which would be about twice as high as the steel pipelines currently in operation.

GPR testing of buried GFRP and PVC pipes have shown that, the use of carbon fabric and aluminum foil overlays on non-metallic pipes (in the form of rings and strips) improves the detectability of such pipes when buried. The addition of carbon fabric or aluminum foil overlays makes the otherwise non detectable non-metallic pipes detectable, producing significantly stronger GPR reflection signals during testing. The production of strong and easier to interpret signals from buried non-metallic pipes with carbon fabric or aluminum foil overlays also implies that, the depth of pipe burial can be increased beyond the 4 ft. maximum depth used in this research and still obtain adequate signal strength using GPR.

By comparing GPR signal reflections from the buried pipes, carbon fabric overlays were observed to produce stronger signals compared to aluminum foil overlays. Additionally, it was observed that carbon fabric and aluminum foil “strips” bonded to the top of the pipes generally produce better/stronger signals compared to carbon fabric and aluminum foil “rings” around non-metallic pipe sections.

Through the IRT test conducted in this research it was concluded that buried pipe transporting hot liquid such as petroleum products from production wells or refinery plants have the potential

of being detectable using IRT. The results showed that, IRT can be used to detect 3" CFRP pipe up to a depth of 16.5" in the test medium used in this research when water at a temperature of 95°C is pumped through the pipe. IRT therefore has the potential of being used in detecting pipelines transporting hot liquids, but the depth of detection will depend on the diameter of the pipe and the temperature of liquid being transported.

The gas leak detection experiments using a Mass Spectrometer showed that experimental “K” values from all the trials in gas leak detection were within five percent of the theoretical value. This is more than acceptable and will become beneficial when a model for the gas flow through the soil is developed. It can also help to estimate the size of a leak in a test section of composite pipe. It can be concluded from the gas leak detection test that the mass flow rate out of the test pipe is in good agreement with the choked flow model and its assumptions. This will help create the one-dimensional diffusion model that will help determine the relationship between the diffusion of gas through the soil and the various levels of soil depth and compaction. A one-dimensional transient diffusion model can be used to fit the experimental data. This part of the research will also allow the back calculation of the size of the leak in the pipe if needed. The other conclusion that can be made is that we have a viable method for detecting a leak with the mass spectrometer with the increase in gas concentration inside the soil.

REFERENCES

- Akovali, G. (2001). *Handbook of Composite Fabrication*. Shawbury: Rapra Technology Limited.
- Baker (2009). Mechanical Damage - FINAL REPORT. Retrieved Aug. 30, 2017, from https://primis.phmsa.dot.gov/gasimp/docs/Mechanical_Damage_Final_Report.pdf, Michael Baker Jr., Inc.
- Dispennette, D. (2012). *Bending, Crushing, and Connector Behavior of Pultruded Glass FRP Tubes*. M.S. Thesis, Dept. of Civil and Environmental Engineering, Morgantown, WV.
- EIA (n.d.). *Primary Energy Consumption by Source*. Retrieved August 30, 2017, from <https://www.eia.gov/totalenergy/data/browser/?tbl=T01.03#/?f=A&start=1949&end=2014&charted=1-2-3-5-12>
- GangaRao, H. V., Halabe, U. B., and Zondlo, J. (2016). *Glass-Polymer Composite High Pressure Pipes and Joints - Design, Manufacture & Characterize*. Research Contract No. DTPH5616HCAP02 awarded by USDOT-PHMSA to Constructed Facilities Center, West Virginia University, Morgantown, WV.
- GangaRao, H., Taly, N., & Vijay, P. (2007). *Reinforced Concrete Design with FRP Composites*. Boca Raton: Taylor and Francis Group.
- Groeger, L. (2012). *Pipelines Explained: How Safe are America's 2.5 Million Miles of Pipelines?* Retrieved August 31, 2017, from <https://www.propublica.org/article/pipelines-explained-how-safe-are-americas-2.5-million-miles-of-pipelines>
- PHMSA (2015). Funding Opportunity Announcement (FOA). In *Pipeline Safety Research Competitive Academic Agreement Program (CAAP)*.
- PHMSA (2016a). *Preliminary Factual Report - Plains Pipeline, LP, Failure on Line 901*.
- PHMSA (2016b). *Failure Investigation Report - Plains Pipeline, LP, Line 901*.
- Rawls, G., and Adams, T. (2014). *Fiber Reinforced Composite Pipelines*. Retrieved from https://www.hydrogen.energy.gov/pdfs/review14/pd022_rawls_2014_o.pdf
- USDOT (n.d.). *Table I-61: Crude Oil and Petroleum Products Transported in the United States by Mode* | Bureau of Transportation Statistics. Retrieved August 30, 2017, from https://www.rita.dot.gov/bts/sites/rita.dot.gov/bts/files/publications/national_transportation_statistics/html/table_01_61.html